Journal of Autoimmunity 144 (2024) 103181

Contents lists available at ScienceDirect

Journal of Autoimmunity

journal homepage: www.elsevier.com/locate/jautimm

A reverse translational approach reveals the protective roles of *Mangifera indica* in inflammatory bowel disease

Anella Saviano [a,1], Anna Schettino [a,1], Nunzia Iaccarino [b], Adel Abo Mansour [c], Jenefa Begum [d], Noemi Marigliano [a], Federica Raucci [a], Francesca Romano [b], Gelsomina Riccardi [b], Emma Mitidieri [b], Roberta d'Emmanuele di Villa Bianca [b], Ivana Bello [b], Elisabetta Panza [b], Martina Smimmo [b], Valentina Vellecco [b], Peter Rimmer [d,e], Jonathan Cheesbrough [d,f], Zhaogong Zhi [d], Tariq H. Iqbal [e,g], Stefano Pieretti [h], Vincenzo Maria D'Amore [b], Luciana Marinelli [b], Valeria La Pietra [b], Raffaella Sorrentino [b], Luisa Costa [i], Francesco Caso [i], Raffaele Scarpa [i], Giuseppe Cirino [b], Antonio Randazzo [b], Mariarosaria Bucci [b], Helen Michelle McGettrick [j,2], Asif Jilani Iqbal [a,d,2,**], Francesco Maione [a,2,*]

[a] *ImmunoPharmaLab, Department of Pharmacy, School of Medicine and Surgery, University of Naples Federico II, Via Domenico Montesano 49, 80131, Naples, Italy*
[b] *Department of Pharmacy, School of Medicine and Surgery, University of Naples Federico II, Via Domenico Montesano 49, 80131, Naples, Italy*
[c] *Department of Clinical Laboratory Sciences, College of Applied Medical Sciences, King Khalid University, Abha, Saudi Arabia*
[d] *Institute of Cardiovascular Sciences (ICVS), College of Medical and Dental Sciences, University of Birmingham, Birmingham, B15 2TT, UK*
[e] *Department of Gastroenterology, Queen Elizabeth Hospital Birmingham NHS Foundation Trust, Birmingham, UK*
[f] *Department of Gastroenterology, Birmingham Heartlands Hospital, University Hospitals Birmingham NHS Foundation Trust, Birmingham, UK*
[g] *Institute of Microbiology and Infection (IMI), College of Medical and Dental Sciences, University of Birmingham, Birmingham, B15 2WB, UK*
[h] *National Center for Drug Research and Evaluation, Istituto Superiore di Sanità, Viale Regina Elena 299, 00161, Rome, Italy*
[i] *Rheumatology Research Unit, Department of Clinical Medicine and Surgery, University of Naples Federico II, via S. Pansini 5, 80131, Naples, Italy*
[j] *Institute of Inflammation and Ageing (IIA), College of Medical and Dental Sciences, University of Birmingham, Birmingham, B15 2WB, UK*

ARTICLE INFO

Keywords:
$CD4^{+}CD45RB^{high}$ colitis
Functional food
IBD
Mangifera indica L.
Nutraceuticals
Th17
Treg

ABSTRACT

Inflammatory bowel diseases (IBDs) are chronic intestinal disorders often characterized by a dysregulation of T cells, specifically T helper (Th) 1, 17 and T regulatory (Treg) repertoire. Increasing evidence demonstrates that dietary polyphenols from *Mangifera indica* L. extract (MIE, commonly known as mango) mitigate intestinal inflammation and splenic Th17/Treg ratio. In this study, we aimed to dissect the immunomodulatory and anti-inflammatory properties of MIE using a reverse translational approach, by initially using blood from an adult IBD inception cohort and then investigating the mechanism of action in a preclinical model of T cell-driven colitis. Of clinical relevance, MIE modulates TNF-α and IL-17 levels in LPS spiked sera from IBD patients as an *ex vivo* model of intestinal barrier breakdown. Preclinically, therapeutic administration of MIE significantly reduced colitis severity, pathogenic T-cell intestinal infiltrate and intestinal pro-inflammatory mediators (IL-6, IL-17A, TNF-α, IL-2, IL-22). Moreover, MIE reversed colitis-induced gut permeability and restored tight junction functionality and intestinal metabolites. Mechanistic insights revealed MIE had direct effects on blood vascular endothelial cells, blocking TNF-α/IFN-γ-induced up-regulation of COX-2 and the DP2 receptors. Collectively, we demonstrate the therapeutic potential of MIE to reverse the immunological perturbance during the onset of colitis and dampen the systemic inflammatory response, paving the way for its clinical use as nutraceutical and/or functional food.

* Corresponding author.
** Corresponding author. Institute of Cardiovascular Sciences (ICVS), College of Medical and Dental Sciences, University of Birmingham, Birmingham, B15 2TT, UK
E-mail addresses: a.j.iqbal@bham.ac.uk (A.J. Iqbal), francesco.maione@unina.it (F. Maione).
[1] These authors share first authorship.
[2] These authors share co-senior authorship.

https://doi.org/10.1016/j.jaut.2024.103181
Received 26 November 2023; Received in revised form 5 February 2024; Accepted 10 February 2024
Available online 23 March 2024

Abbreviations

BVEC	blood vascular endothelial cells
CD	Crohn's disease
cLP	colonic lamina propria
COX-2	cyclooxygenase-2
DMSO	dymethyl sulfoxide
DP	prostaglandin D_2 receptor
EC	endothelial cell
EDTA	ethylenediaminetetraacetic acid
ELISA	Enzyme-linked immunosorbent assay
Enro/metro	Enrofloxacin/Metronidazole
FBS	fetal bovine serum
FITC	fluorescein isothiocyanate
GALT	gut-associated lymphoid tissue
HBSS	Hanks' balanced salt solution
HDBECs	human dermal blood endothelial cells
HUVEC	human umbilical vein-derived endothelial cells
IBD	inflammatory bowel disease
IBS	irritable bowel syndrome
IFN-γ	interferon-gamma
IL	interleukin
IMIDs	immune-mediated inflammatory diseases
i.p.	intraperitoneally
LPS	lipopolysaccharides
LVEC	lymphatic vascular endothelial cells
MIE	*Mangifera indica* L. extract
mPGES	microsomal prostaglandin E synthase
NF-κB	nuclear factor-kappa B
NSAIDs	nonsteroidal anti-inflammatory drugs
PBLs	peripheral blood lymphocytes
PBMCs	peripheral blood mononuclear cells
PBS	phosphate-buffered saline
PG	prostaglandin
p.o.	orally
SCFA	short-chain fatty acids
Th	T helper
TNF-α	tumor necrosis factor alpha
Treg	regulatory T cells
UC	ulcerative colitis
ZO-1	zona occludens-1.

1. Introduction

Inflammatory bowel disease (IBD), including ulcerative colitis (UC) and Crohn's disease (CD), are chronic debilitating conditions with an increasing incidence and prevalence globally [1,2]. There are many factors thought to lead to the development of colitis, including persistent intestinal inflammation (related to age, gender, and genetics factors), diet, alterations in the function of gut microbiota and immune system homeostasis, all of which are interlinked [3]. Whilst the aetiology and pathogenesis are not yet fully known [4], it seems that persistent intestinal inflammation may result from a dysregulated immune response to mucosal antigens involving a variety of cells with pathogenic and regulatory properties [5]. Among them, T helper (Th) cells (mainly Th1 and Th17) and regulatory T (Treg) cells play a crucial role in the perpetuation and maintenance of self-tolerance in IBD, respectively [6].

Despite the lack of specific dietary advice in IBD, more than 70% of sufferers note that inadequate nutrition significantly affects the course of the disease and increases the frequency and severity of symptoms [7]. Consequently, patients with UC often seek nutritional guidance to help improve their quality of life and contribute to symptom relief [7,8]. Unfortunately, studies to date do not provide a solid basis for creating strong evidence-based dietary recommendations [9]. Whether dietary supplements and/or nutraceuticals are effective against colonic inflammation and immune dysregulation remains an open area of active investigation [10]. Recently, a growing body of studies has indicated that phytochemicals derived from natural products are potent regulators of Th17/Treg repertoire and exert preferable protective benefits against colonic inflammation [11]. This "immunological hypothesis" has attracted increasing scientific evidence, and it may represent the "turning key" for IBD-related dietary recommendations and the rationale for the specific use of herbal-based preparation/formulation in disease onset and/or progression [12,13].

Recent research has demonstrated the relevance of *Mangifera indica* L. extract (here referred as MIE, and commonly known as mango) polyphenols (mainly the glucosylxanthone mangiferin) in the prevention of chronic inflammatory diseases, including IBD [14,15]. Mangiferin possesses prominent anti-inflammatory and immunomodulatory properties thanks to its capacity to decrease $CD4^+IL\text{-}17^+$ cells (Th17 phenotype) maturation [16] and to promote the development of $CD3^+CD25^-$ T cells into $CD4^+FOXP3^+$ cells (Treg phenotype) by suppressing the mTOR activation pathway [17]. In parallel, studies on DSS- and TNBS-induced experimental colitis in mice revealed that an oral supplement with *Mangifera indica* L. and/or its active component(s) effectively ameliorates colonic inflammation through nuclear factor-kappa B (NF-κB) and MAPK signalling inhibition [18] and by the restoration of altered Th17/Treg cells physiological ratio [16,19]. In other disease settings, such as gouty arthritis, we have also shown the ability of MIE to ameliorate inflammation related to clinical and biochemical parameters [20].

The current relevant literature demonstrates a protective role for mangiferin or *Mangifera indica* L. extract in experimental IBD, but these studies are limited to the observation of an association between mangiferin-induced modulations in gut immunoinflammatory state and the disease outcome. Notably, no single animal model completely recapitulates the clinical and histopathological characteristics of human IBD, considering that chronic gut inflammation, largely mediated by T lymphocytes and the presence of commensal enteric bacteria, are detrimental to the initiation and perpetuation of intestinal and/or colonic inflammation. These features are required to mimic the human disease [21]. Thus, conclusive evidence is lacking to connect the mechanism of action of mangiferin in clinically relevant models of IBD (in both preclinical and clinical assessments) and a full understanding of its anti-inflammatory and immunomodulatory properties.

With this rationale, we explored the therapeutic potential of a *Mangifera indica* L. extract (MIE; at 90% purity of mangiferin) by taking a reverse translational approach, initially using blood from an adult IBD inception cohort and then investigating the mechanism of action in a preclinical model of T cell-driven colitis. Our investigation demonstrates the potent action of MIE in ameliorating inflammatory mediator release from lipopolysaccharides (LPS)-stimulated blood taken from CD, Irritable Bowel Syndrome (IBS) and UC patients and, preclinically, to reverse disease severity and intestinal inflammation. Mechanistically, we show MIE regulates the trafficking of the inflammatory infiltrate through the cyclooxygenase-2 (COX-2)-prostaglandin D_2 receptor (DP)2 signalling pathway *in vitro* and *in vivo*. Collectively, these data highlight *Mangifera indica* L. extract and its main active constituent mangiferin as a natural therapeutic agent [22] with the potential to treat a broad range of immune-mediated inflammatory diseases (IMIDs).

Table 1
Demographic, clinical and laboratory characteristics of IBD patients.

	UC (N = 10)	CD (N = 11)	IBS (N = 9)	Transient infection (N = 1)	Other GI (N = 4)
Age (years)[a]	31.50 (26–43)	33 (24–43)	33 (20–41.5)	60	36 (25.75–44)
Female; number (%)	5 (50)	9 (81.82)	7 (77.78)	0 (0)	2 (50)
Ethnicity White; number (%)	9 (90)	7 (63.64)	5 (55.56)	1 (100)	3 (75)
Symptom duration (months)[a]	5 (2–12)	10.5 (4.75–18)	6 (2–12)	1	5 (2–8)
Weight (kg)[a]	70.50 (64.90–74.30)	67.70 (58.48–81.45)	72 (59.7–79.95)	87	79.55 (73.40–85.70)
Height (m)[a]	1.69 (1.63–1.75)	1.61 (1.56–1.69)	1.66 (1.59–1.69)	1.73	1.64 (1.63–1.65)
BMI [a]	24.57 (22.44–25.55)	27.13 (21.89–31.80)	27.65 (21.56–29.91)	29.07	30.39 (27.63–33.15)
Smoker; number (%)	2 (20)	1 (9.09)	1 (11.11)	0 (0)	1 (25)
FCAL at baseline (μg g^{-1})[b]	1057 ± 876.10	1047 ± 838.30	652.80 ± 657.70	174 ± 0	1067 ± 1093
CRP (mg/l)[a]	2 (1.25–3)	6 (1–12)	1 (1–3)	24	4 (1–7)
HBI[a]	na	10 (6–11.75)	na	na	na
Partial Mayo[a]	4 (2.75–6)	na	na	na	na
Endoscopic Mayo[a]	1 (1–2)	na	na	na	na
SES-CD[a]	na	7 (3.5–11)	na	na	na
Montreal Classification; Extent/Location (%)	E1: 2 (20%) E2: 2 (20%) E3: 6 (60%)	L1: 5 (45.4%) L2: 3 (27.3%) L3: 3 (27.3%)	na	na	na
Montreal Classification; Severity/Behaviour (%)	S1: 7 (70%) S2: 3 (30%) S3: 0	B1: 8 (72.7%) B2: 1 (9.1%) B3: 2 (18.2%)			
Treatments utilised (initiated after sampling)	5-ASA: 10 Prednisolone: 2 Immunomodulator: 1 Biologics: 1	5-ASA: 1 Budesonide: 5 Prednisolone: 4 Immunomodulator: 2 Biologics/small molecules: 5 Surgery: 1	–	–	–

Categoring race and ethnicty = White, Asian and Black.
[a] median (interquartile range).
[b] mean ± SD; BMI=Body Mass Index; CD=Crohn's disease; CRP = C- reactive protein; FCAL = faecal calprotectin; HBI=Harvey-Bradshaw Index; IBS = irritable bowel syndrome; na = not applicable; SES-CD=Simple Endoscopic Score for Crohn's disease; UC=Ulcerative colitis; 5-ASA = 5-aminosalicylic acid; - = data not obtained from patients at time of presentation.

2. Materials and methods

2.1. Reagents and chemicals

Mangifera indica L. extract (MIE, 90% mangiferin, batch number: CMGD-C-A091434) was supplied and certified by L.C.M. Trading S.p.A. (Milan, Italy) and chemically characterized in our previous study [20]. Dimethyl sulfoxide (DMSO), ethanol, fetal bovine serum (FBS), glutaraldehyde, histopaque®-1077, KH_2PO_4, K_2HPO_4, LPS from *Escherichia coli* (O55:B5, c.n.: L5418), TSP and NaN_3 were purchased from Sigma-Aldrich Co. (now under Merck, Darmstadt, Germany). ACK Lysing Buffer, Medium 199 and RPMI-1640 cell medium were obtained from Gibco Invitrogen Compounds (Paisley, Scotland). Enrofloxacin and metronidazole (Enro/Metro) were purchased by CliniSciences (Nanterre, France), while *in vivo* MAb anti-tumor necrosis factor alpha (TNF-α; c.n. XT3.11) from BIO X Cell (Lebanon, USA). For flow cytometry analysis, fixation and permeabilization buffer were purchased from ThermoFisher Scientific (Carlsbad, CA), while FACS buffer and conjugated antibodies were from BioLegend (London, UK). For Western blot antibodies, rabbit polyclonal IgG claudin-2 was obtained from Biorbyt (Cambridge, UK), goat polyclonal IgG COX-2 and rabbit polyclonal IgG microsomal prostaglandin E synthase (mPGES)-1 from Novus Biologicals (Milan, Italy), rabbit polyclonal IgG occludin and rabbit polyclonal IgG zona occludens-1 (ZO-1) were obtained from Proteintech (Manchester, UK), rabbit polyclonal IgG DP1 from Elabscience (Milan, Italy), whereas rabbit polyclonal IgG DP2 and rabbit polyclonal anti-beta-actinfrom Origene (Maryland, US). HRP-conjugated IgG secondary antibodies were purchased from Dako (Copenhagen, Denmark). Unless otherwise stated, all the other reagents were from BioCell (Milan, Italy).

2.2. Ethics approval

Informed consent was provided according to the Declaration of Helsinki. This study was approved by the University of Birmingham Local Ethical Review Committee (ERN_18–0382; RG_21–009 and ERN_12–0079). An equal proportion of male and female donors were used with an age range between 19 and 60 (Table 1) [23].

2.3. Ex vivo whole blood assay

Blood was collected from adult patients with UC (N = 10), CD (N = 11) and IBS (N = 9). Patients were recruited from the gastroenterology Department of Queen Elizabeth Hospital and Birmingham Heartlands Hospital (Birmingham, UK) and their diagnosis was established by standard clinical, endoscopic and histologic criteria [24]. All subjects were treatment-naïve, not receiving any form of medication (glucocorticoid or nonsteroidal anti-inflammatory drugs, NSAIDs) at the time the blood was taken [25] (Table 1). Since patients are in the early stages of evaluation and diagnosis, the stage of disease or the status of remission has not been determined at the point of inclusion into this study. Whole blood culture and stimulation were performed as described by Papandreou and coll., with small modifications [26]. Briefly, whole venous blood, collected into lithium heparin tubes, from patients with clinically

diagnosed IBS and IBD was placed in 96-well plates and pre-treated with MIE extract (0.03–10 μg ml^{-1}) or corresponding vehicle (DMSO at the highest concentration used in test wells, 0.25%) for 1 h before stimulation with or without LPS (0.1 μg ml^{-1}) for 3 h at 37 °C. The selected range of concentrations of MIE was based on our previous study [20]. After the incubation period, the culture plate was briefly centrifuged (300 g, 5 min at RT), and the sera obtained were assessed for the analysis of TNF-α and interleukin (IL)-17 levels according to the procedure previously described [23,26].

2.4. Animals

All animal care and experimental procedures complied with reporting of *in vivo* experiments (ARRIVE) guidelines, international and national law and policies and were approved (Authorisation number: 533/2021-PR) by the Italian Ministry of Health (EU Directive 2010/63/EU for animal experiments, and the Basel declaration including the 3Rs concept). Male BALB/c and immunodeficient RAG1 KO mice were purchased respectively from Charles River (Milan, Italy) and Jackson Laboratories (Bar Harbon, USA). Animals were housed under specific pathogen-free conditions in ventilated cages under controlled temperature and humidity, on a 12 h light/dark cycle and allowed *ad libitum* access to standard laboratory chow diet and sterile water. Experimental study groups were randomized, and their assessments were carried out by researchers blinded to the treatment groups.

2.5. T-cell transfer model of colitis

Adoptive transfer of $CD4^+CD45RB^{high}$ T cells (naïve T cells) from healthy donor mice (BALB/c) into RAG1 KO recipient mice induced colitis approximately 4–7 weeks following the T cell transfer. Histopathological inspection of the colon from mice with active disease reveals similar pathology findings in IBD patients [21,27]. $CD4^+$ T cell subsets were isolated from the spleen of BALB/c mice as described previously [28]. Briefly, a single-cell suspension was prepared, smashing spleens through a 40 μm cell strainer and lysing red blood cells with ACK buffer [29]. $CD4^+$ T cells were first isolated using the anti-CD4 (L3T4)-MACS system (Miltenyi Biotec, Germany) according to the manufacturer's instructions. Enriched $CD4^+$ T cells (96–97% pure) were then labelled with CD4 (1 μg ml^{-1}; clone RM4-5, c.n.: 17-0042-82), CD25 (1 μg ml^{-1}; clone 7D4, c.n.: 558642) and CD45RB (2.5 μg ml^{-1}; clone 16A, c.n.: 553100) antibodies (all from BD Biosciences) for 20 min at 4 °C. $CD4^+CD25^-CD45RB^{high}$ cells fraction was purified, under sterile conditions, using a FACS Aria Fusion cell sorter (BD Biosciences, California, USA) [30,31]. The purity of cell isolates was confirmed by flow cytometry analysis. The $CD45RB^{high}$ and $CD45RB^{low}$ populations were defined as the brightest staining 40–60%, and the dullest staining 15–20% $CD4^+$ T cells, respectively [28] (Supplementary Fig. 1). Thereafter, each recipient mouse was injected intraperitoneally (i.p.) with 0.5×10^6 naïve colitogenic T cells in 500 μl of sterile PBS [32,33] and the body weight was monitored three times weekly for 7 weeks, according to the procedures previously described [34]. RAG1 KO mice were administrated with MIE (10 mg kg^{-1}), anti-TNF-α MAb (25 mg kg^{-1}; clone XT3.11, rat IgG1, c.n.: BE0058), antibiotic mix Enrofloxacin/Metronidazole (Enro/metro; 380/875 mg kg^{-1}, c.n.: HY-B0502 and HY-B0318 respectively), and corresponding vehicle (DMSO/saline 1:3 w/w as the minimum concentration required to enable solubilization and to devoid any anti-inflammatory activity *per se*, [35]) from week 3, after adoptive transfer, to week 7. MIE, Enro/metro or vehicle were administered once daily orally (p.o.) by oral gavage, while anti-TNF-α was injected i.p. twice a week. The route, timing, and frequency of administration, as well as the selected dosages of MIE and tested compounds, were selected according to updated literature [20,36]. Colons and spleens were harvested at the experimental endpoint (7 weeks), and length was measured and weighed [37]. Specifically, the colon was resected between the ileocecal junction and the proximal rectum, and its length was measured [38]. The obtained samples were stored at −80 °C and used for further *ex vivo* analysis.

2.6. Clinical observation

All mice were observed for clinical signs and, at autopsy, the clinical score was assessed by three investigators who were blinded to the experimental conditions. Clinical score was assessed by the sum of three parameters as follows: hunching and wasting, 0 or 1; colon thickening and/or inflammation score (0, no colon thickening and/or no inflammation; 1, mild thickening and/or local hyperemia without ulceration; 2, moderate thickening and/or ulceration without hyperemia; 3, extensive thickening and/or one or more sites of ulceration and inflammation); and stool consistency score (0, normal beaded stool; 1, soft stool; 2, diarrhoea; 3, bloody stool) accordingly to previous studies [31,39].

2.7. Isolation of colonic epithelial and lamina propria (cLP) cells and splenocytes

Colonic epithelial cells were isolated from colonic specimens according to previously described protocols [40,41]. Briefly, colons were removed and flushed several times with ice-cold PBS to remove intestinal content opened longitudinally and cut into small segments. Tissues were then incubated three times with pre-warmed cell dissociation solution made with Hanks' balanced salt solution (HBSS), 5% FBS, ethylenediaminetetraacetic acid (EDTA) 2 mM, and HEPES 10 mM for 30 min at 37 °C. After incubations, epithelial cells were dislodged by vigorous shaking, harvested by centrifugation (500 g, 5 min at 4 °C) and analysed by Western blot for tight junction expression as described below [42]. Subsequently, to obtain colonic lamina propria (cLP) cells, colonic pieces were minced and treated with a digestion cocktail containing 1.5 mg ml^{-1} collagenase type IV (c.n.: C5138, Sigma-Aldrich Co.) and 0.1 mg ml^{-1} DNase I (c.n.: LS006342, Worthington-Biochem, New Jersey, USA) in RPMI 1640/10% FBS for 45 min at 37 °C with continuous stirring [32,43,44]. cLP cells were then filtered through a cell strainer with a 70-μm nylon mesh (Biologix, Ohio, USA) and washed with RPMI 1640/10% FBS, whereas splenocytes were isolated from the spleens in phosphate-buffered saline (PBS) and passed through a 40 μm-mesh-sized cell strainer (Corning, Arizona, USA) to obtain single cells after lysing of red blood cells by ACK buffer [45]. Collected cells (cLP and splenocytes) were washed in PBS for total cell count before flow cytometry analysis. Cell number was determined by TC20 automated cell counter (Bio-Rad, Milan, Italy) using Bio-Rad's disposable slides, TC20 trypan blue dye (0.4% trypan blue dye w/v in 0.81% sodium chloride and 0.06% PBS) and a CCD camera to count cells based on the analyses of capture images [20,46].

2.8. Flow cytometry analysis

Cells collected from digested colon tissues (cLP cells) and splenocytes were washed in FACS buffer (PBS containing 1% BSA and 0.02% NaN_2) and directly stained with the following conjugated antibodies (all from BioLegend, London, UK): CD4 (1:200; clone GK1.5, c.n.: 100405) and CD25 (1:200; clone 3C7, c.n.: 101911) for 60 min at 4 °C. After washing, cells were fixated, permeabilized, and stained intracellularly with interferon-gamma (IFN-γ; 1:200; clone XMG1.2, c.n.: 505807), IL-17A (1:200; clone TC11–18H10.1, c.n.: 506903) and FOXP3 antibody (1:200: clone MF-14, c.n.: 126403). Th1, Th17 and Treg populations were defined as $CD4^+$IFN-γ^+, $CD4^+$IL-17^+ and $CD4^+CD25^+FOXP3^+$ cells respectively, according to the flow cytometry procedure previously described [20,47,48]. At least 1×10^4 cells were analysed per sample, and positive and negative populations were determined based on the staining obtained with related IgG isotypes. Flow cytometry was performed on BriCyte E6 flow cytometer (Mindray Bio-Medical Electronics, Nanshan, China) using MRFlow and FlowJo software operation [49,50].

Flow cytometry strategy for cLP cells and splenocytes is reported in Supplementary Fig. 2 and Supplementary Fig. 3, respectively.

2.9. Determination of faecal water and calprotectin levels

Fresh stools were collected at indicated time points (weeks 1–7 after T-cell transfer) into pre-tared 1.5 ml tubes and immediately sealed. After weighing, tubes were uncapped and completely desiccated by incubation in a dry oven at 60 °C for 24 h. Tubes were then re-weighed, and faecal water was determined as the percentage of total water lost upon desiccation [42]. To provide samples for the calprotectin Elisa assay, dried stools were rehydrated with 5x the initial water volume and homogenized in extraction buffer (95% ethanol) for 25 min. After centrifugation (1100 g, at RT) for 10 min to insoluble pellet debris, the calprotectin content of the supernatant was measured by Elisa (c.n.: E-EL-M1143, Elabscience) [51].

2.10. Intestinal permeability assay

Mice were denied access to food but allowed water for 3 h before gavage with 0.2 ml of PBS (pH 7.49) containing 22 mg ml^{-1} permeability tracer fluorescein isothiocyanate (FITC)-4 kDa dextran (c.n.: 4013, Chondrex, Inc., Woodinville, USA) [52]. Blood samples were obtained by an intracardiac puncture after 3 h and centrifugated (1000 g, at 4 °C) for 20 min. For use as measurement, harvested sera (light protected), mixed with an equal volume of PBS, freshly prepared standards as well as blanks (PBS and diluted sera from untreated animals) were transferred to a black 96-well microplate. Analysis of the FITC-4 kDa dextran was carried out with a fluorescence spectrophotometer (GloMax® Explorer microplate reader, Promega) using excitation wavelengths of 490 nm and emission wavelengths of 520 nm [53].

2.11. Metabolites extraction for NMR analysis

Faecal samples (30 mg) were re-suspended in milliQ water, at a faecal weight to the water volume of ratio 1:2 and extracted by mixing with phosphate buffer prepared as described below. Briefly, 1.5 M solutions of KH_2PO_4 and K_2HPO_4 were prepared in milliQ water and mixed using magnetic stirrers at RT until complete dissolution. The two solutions, KH_2PO_4 and K_2HPO_4 were mixed in a 1:4 (vol:vol) ratio. Then, TSP and NaN_3 were added to the phosphate buffer at concentrations of 1 mg ml^{-1} and 0.13 mg ml^{-1}, respectively. The obtained solution was mixed using magnetic stirrers at RT for 10 min and stored overnight to ensure pH equilibration. 100 ml of this buffer was mixed with 900 ml of milliQ water to obtain the buffer used in this analysis [54]. After centrifugation (14000 g, at 37 °C) for 30 min, the supernatants were collected for NMR measurements.

2.11.1. NMR spectroscopy

A total of 65 μL of D_2O was added to the faecal extracts, vortexed briefly and transferred into 5-mm NMR tubes. All one-dimensional ^1H NMR spectra were acquired at 298 K on a Bruker Avance NEO 600 MHz spectrometer (Bruker Biospin Gmbh, Rheinstetten, Germany) equipped with a QCI cryo-probe set for 5 mm sample tubes and an autosampler (SampleJet). The ^1H NMR spectra of faecal extracts were acquired with Topspin 4.1 (Bruker Biospin GmbH, Rheinstetten, Germany), using the 'noesygppr1d' pulse sequence allowing for a quantitative evaluation even close to the water signal, which was presaturated at 4703 ppm. NMR samples were stabilized at 298 K for 300 s, inside the probe, before starting the experiment. An acquisition time of 2.62 s, a relaxation delay of 4 s, receiver gain of 101, 32 scans, 4 dummy scans and a spectral width of 12500.0 Hz (208287 ppm) were employed. All samples were automatically tuned, matched, and shimmed. Prior to Fourier transformation, the free induction decays were multiplied by an exponential function equivalent to a 0.3-Hz line-broadening factor. Then, the transformed spectra were automatically corrected for phase and baseline distortions and calibrated using TopSpin built-in processing tools. The assignment of the metabolites was achieved by (i) analysis of literature data [54–56]; (ii) comparison with the chemical shifts of the metabolites in the Human Metabolome Database (HMDB); (iii) peak fitting routine within the spectral database in Chenomx NMR Suite 8.4 software package (Chenomx, AB, Canada) in its evaluation version.

2.11.2. NMR Data Reduction and Processing

NMR spectra were then imported into MATLAB (R2015b; Mathworks, Natick, Massachusetts, USA) where the spectral regions above 10 ppm and below 0 ppm were removed because they contained only noise. To correct for spectral misalignment, an interval-based alignment step was carried out using the icoshift algorithm [57] and choosing the acetate singlet at 1.90 ppm as the reference signal. Then, to reduce the model complexity, the peak areas of the well-separated and safely assigned resonances of 22 selected metabolites were manually integrated and submitted to the data analysis as a data matrix made of 12 rows (samples) x 22 columns (metabolites). Such data matrix was then submitted to the PLS toolbox version 8.6.1 (Eigenvector Research, Manson, Washington, USA) under MATLAB environment to perform Principal Components Analysis (PCA). Prior to the analysis, data was normalized, according to the total area (1-Norm) and then autoscaled. Autoscaling employs both the standard deviation as a scaling factor thus giving all metabolites the same chance to affect the model and the mean-centring, which is needed to compute PCA.

2.12. Preparation of colonic tissue homogenates

Portions of colons (0.5 cm) were homogenized in ice-chilled Tris-HCl buffer (20 mM, pH 7.4) containing 0.32-M sucrose, 1 mM EDTA, 1 mM EGTA, 1 mM PMSF, 1 mM sodium orthovanadate, and one protease inhibitor tablet per 50 ml of buffer, sonicated on ice and centrifuged (4500 g, at 4 °C) for 10 min. Total proteins within the supernatants were quantified using a Bradford protein assay (Bio-Rad) [58]. Supernatants were assayed for prostaglandin (PG)E_2 and PGD_2 Elisa kits and PTGDR1 (also referred as DP1) and PTGDR2 (also referred as DP2) Western blot analysis and quantified by Multiplex cytokine assay according to manufacturer's directions [59].

2.13. Multiplex cytokine assay

The concentrations of Th-related cytokines from colon tissue homogenates were determined using the multi-LEGENDplex™ analyte flow assay kit (mouse Th Panel (12-plex), c.n.: 741043, Biolegend). Briefly, antibodies specific to the 12 analytes were conjugated to 12 different fluorescence-encoded beads. The beads were mixed with the supernatants, incubated for 2 h at RT, washed, and incubated for 1 h with detection antibodies. Finally, streptavidin-PE was added and incubated for 30 min, and the beads were washed and acquired using BriCyte E6 flow cytometer (Mindray Bio-Medical Electronics). The results were analysed by using the Legendplex software (version 8.0) [59].

2.14. Primary human dermal blood endothelial cells

Commercially sourced primary human dermal blood endothelial cells (HDBECs; PromoCell, Heidelberg, Germany) were cultured in endothelial cell growth medium MV. HDBECs were seeded into 12-well tissue culture plates after 4 passages at a seeding density yielding confluent monolayers. HDBEC monolayers were washed in endothelial cell growth medium MV warmed to 37 °C and stimulated with TNF-α (100 U ml^{-1}, c.n.: 210-TA; R&D System, Abingdon, UK) and IFN-γ (10 ng ml^{-1}, c.n.: 300-02, Peprotech, London, UK) in presence of MIE extract (1 μg ml^{-1}) or its corresponding vehicle (DMSO, 0.25%) for 24 h. Supernatants were collected and measured to evaluate PGE_2 and PGD_2 levels, whereas cells were analysed by Western blot as described below [23,60,61].

2.15. Isolation of human peripheral blood lymphocytes (PBLs)

Venous blood from healthy volunteers was collected into 10 ml EDTA-coated tubes. Peripheral blood mononuclear cells (PBMCs) were isolated by centrifugation of blood on histopaque 1077, and peripheral blood lymphocytes (PBLs) were prepared by panning human PBMCs on culture plastic to remove monocytes [62,63]. Isolated cells were washed, counted, and adjusted to a final concentration of 1×10^6/ml in Medium 199, supplemented with 0.15% BSA (Sigma-Aldrich; M199BSA).

2.16. Static adhesion assay

HDBEC were seeded and stimulated with TNF-α (100 U ml^{-1}, R&D System) and IFN-γ (10 ng ml^{-1}, Peprotech) in the presence of MIE extract (0.1–10 μg ml^{-1}) or its corresponding vehicle (DMSO, 0.25%) for 24 h before the assay with lymphocytes. PBLs were isolated from healthy volunteers as described above prior to being added to activated HDBEC for 7 min at 37 °C. Wells were washed twice with PBS to remove unbound cells and fixed with 2% glutaraldehyde for 10 min at RT. Glutaraldehyde was removed with several 1 ml washes of PBS (with Ca^{2+} and Mg^{2+}). Images were taken at five different fields in the centre of each well using phase-contrast microscopy (IX71; Olympus, Tokyo, Japan). Images were analysed offline using Image-pro 7.0 software (Media Cybernetics, Rockville, MD, USA), with adherent cells being defined as phase bright round cells, whilst transmigrated cells were shape changed and phase dark. PBLs adhesion was expressed as the total number of cells per mm^2, while transmigration was expressed as a percentage of transmigrated cells [23,64].

2.17. Western blot analysis

Colonic epithelial cells, colonic tissues, and HDBEC cells were lysed and subjected to SDS-PAGE (10% gel) using standard protocols as previously described [65,66]. The proteins were transferred to nitrocellulose membrane (0.2-μm nitrocellulose membrane, Trans-Blot®TurboTM, Transfer Pack, Bio-Rad Laboratories, Hercules, CA, USA, RRID: SCR_008426) in transfer buffer (25-mM Tris–HCl pH 7.4 containing 192-mM glycine and 20% v/v methanol) at 400 mA for 2 h. Membranes were incubated for 2 h with non-fat dry milk (5% wt/v) in PBS supplemented with 0.1% (v/v) Tween 20 (PBS-T) at RT and then incubated at 4 °C with the appropriately diluted primary antibodies overnight: rabbit polyclonal claudin-2 (1:1000; c.n.: ORB214855), rabbit polyclonal occludin (1:1000; c.n.: 13409-1-AP), rabbit polyclonal ZO-1 (1:1000; c.n.: 21773-1-AP) (for colonic epithelial cell lysates), goat polyclonal COX-2 (1 μg ml^{-1}; c.n.: AF4198), rabbit polyclonal mPGES-1 (1:1000; c.n.: H00009536-D01P), rabbit polyclonal DP1 (1:1000; c.n.: E-AB-65975) and rabbit polyclonal DP2 (1 μg ml^{-1}; c.n.: TA306387) (for both colon and HDBEC lysates). After lavages with PBS-T, blots were incubated with a 1:3000 dilution of related horseradish peroxidase-conjugated secondary antibody for 2 h at RT and finally washed 3 times with PBS-T. Protein bands were detected by using the enhanced chemiluminescence method (Clarity™ Western ECL Substrate, BioRad Laboratories, Hercules, CA, USA) and Image Quant 400 GE Healthcare software (GE Healthcare, Italy). Bands were quantified using the GS 800 imaging densitometer software (Biorad, Italy) and normalized with respective actin (1:1000; c.n.: TA890010) [23,67,68]. Uncropped and triplicate original western blots for colonic epithelial cells, HDBEC cells, and colonic tissues are presented in Supplementary Fig. 4, Supplementary Fig. 5, and Supplementary Fig. 6, respectively.

2.18. Elisa assay

Enzyme-linked immunosorbent assay (ELISA) for PGE_2 (c.n.: KGE004B, R&D Systems) and PGD_2 (c.n.: E-EL-0066; Elabscience) was carried out on colon tissue homogenates and supernatants from human HDBEC cells. TNF-α (c.n.: DY210) and IL-17 (c.n.: DY317) levels in serum from IBD patients were quantified by commercially available kits (both from R&D System) according to the procedure described by Raucci and coll [46]. Briefly, 100 μl of supernatants, diluted standards, quality controls, and dilution buffer (blank) were applied on a plate with the monoclonal antibody for 2 h. After washing, 100 μl of biotin-labelled antibody was added, and incubation continued for 1 h. The plate was washed, and 100 μl of the streptavidin-HRP conjugate was added, and the plate was incubated for a further 30 min period in the dark. The addition of 100 μl of the substrate and stop solution represented the last steps before the reading of absorbance (measured at 450 nm) on a microplate reader (Multiskan™ GO Microplate Spectrophotometer; Thermo Scientific™). Antigen levels in the samples were determined using a standard curve and expressed as pg ml^{-1} [69,70].

2.19. Docking simulations

Molecular docking of mangiferin into the X-ray structures of DP2 (PDB code: 6D27 [71] was carried out using the Glide 5.5 program. Maestro v. 12.7.156 (Maestro, Schrödinger, LLC, New York, NY, 2021) was employed as the graphical user interface, and the most probable binding mode of mangiferin was rendered by the Pymol software package (Schrödinger, L. & DeLano, W., 2020. PyMOL, Available at: http://www.pymol.org/pymol).

2.19.1. Ligand and protein setup

As for the mangiferin structure: the molecule was built and prepared through the LigPrep (LigPrep, Schrödinger, LLC, New York, NY, 2021) module of Maestro, employing the OPLS2005 force field. Epik (Epik, Schrödinger, LLC, New York, NY, 2021) is used to evaluate the ligands' pKa at neutral pH and so to properly describe its protonation state. Then, the obtained ligand is optimized at the molecular mechanics level through the MacroModel (MacroModel, Schrödinger, LLC, New York, NY, 2021) program included in the Schrödinger suite of programs. The target protein was prepared using the protein preparation wizard in Maestro 9.0.211. Water molecules were removed, hydrogen atoms were added, and minimization was performed until the rmsd of all heavy atoms was within 0.3 Å of the crystallographic positions. The binding pocket was identified by placing a 20 Å cube around the co-crystallized ligand. The obtained protein was then processed through the Protein Preparation Wizard of the graphical user interface Maestro and the OPLS-2005 [72] force field.

2.19.2. Docking setting

Molecular docking calculations were performed with the aid of Glide 5.5 in SP mode [73,74], using Glidescore for ligand ranking, letting all the other parameters as default. Sampling of nitrogen atoms inversions (when not belonging to cycles) and of different ring conformations were allowed, while non-planar amide conformations were penalized. The receptor was kept fixed, the ligand was treated as flexible, and no other constraints were added.

2.20. Statistical analysis

Statistical analysis complies with the international recommendations on experimental design and analysis in pharmacology and data sharing and presentation in preclinical pharmacology [20,68]. Data are presented as mean ± S.D or median ± IQR. Normality was tested prior to analysis with one or two-way ANOVA followed by Bonferroni's or Dunnett's for multiple comparisons, where $P \leq 0.05$ was deemed significant. GraphPad Prism 8.0 software (San Diego, CA, USA) was used for analysis. For *in vivo* studies, animal weight was used for randomization and group allocation to reduce unwanted sources of variations by data normalization. No animals and related *ex vivo* samples were excluded from the analysis. The study was carried out to generate groups of equal size ($N = 6$ of independent values) using randomization and blinded analysis.

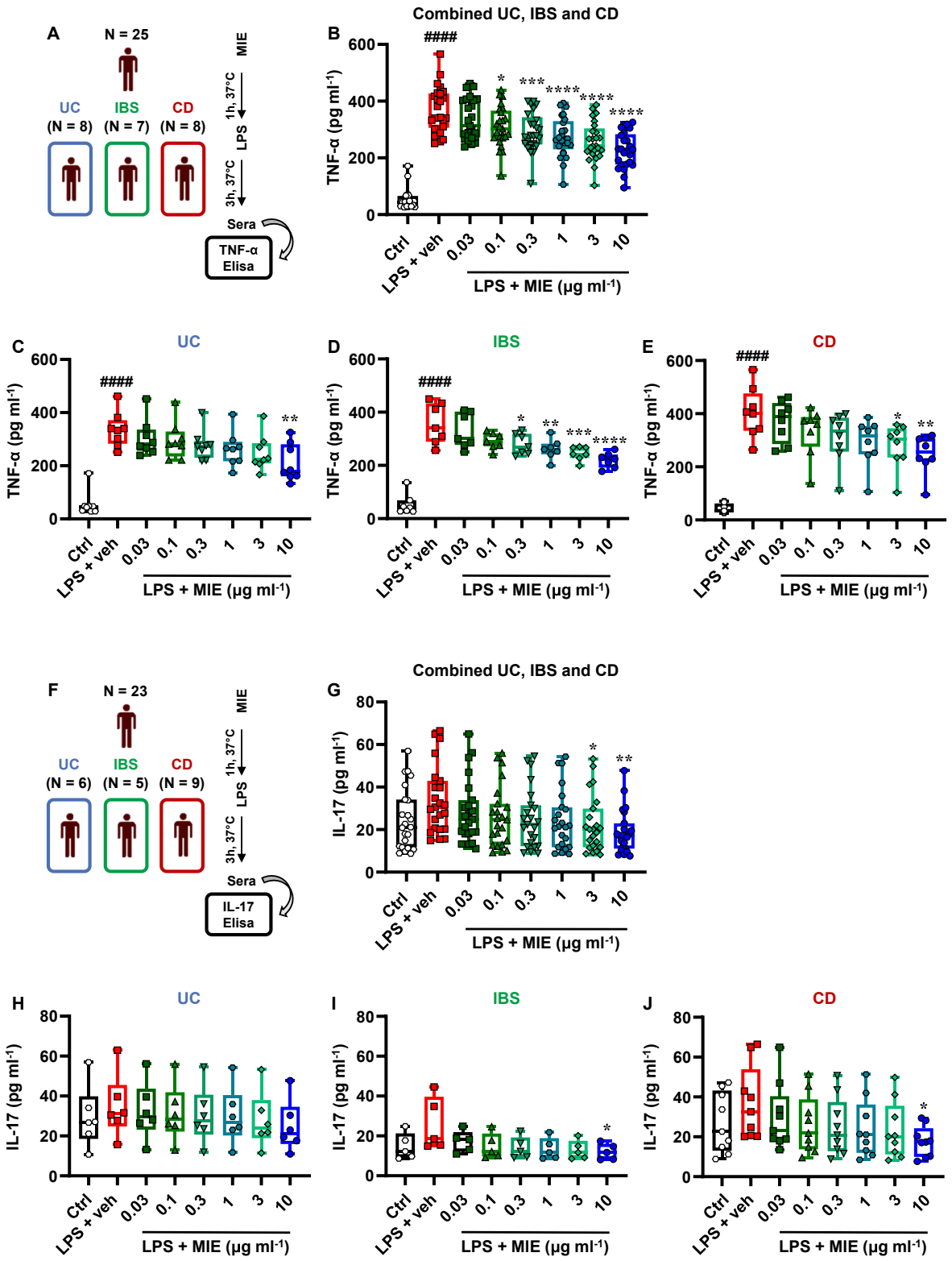

Fig. 1. Translating MIE treatment for human inflammatory bowel disease.
Schematic representation of clinical design and outcomes (**A**, **F**). Disease categories, for patients' stratification, were colour-coded in the outer ring as follows: blue, ulcerative colitis (UC); green, irritable bowel syndrome (IBS) and red, Crohn's disease (CD) (**A**, **F**). Specifically, human whole blood collected from IBD patients was pre-treated with MIE vehicle (veh; DMSO at the highest concentration used in test wells, 0.25%) or MIE extract (0.03–10 μg ml^{-1}) for 1 h before stimulation with LPS (0.1 μg ml^{-1}) for 3 h at 37 °C. Serum was collected for the assessment of TNF-α (**A**–**E**) and IL-17 (**F**–**J**) by ELISA. The study population included three cohorts: patients with UC (N = 6–8), IBS (N = 5–7) and CD (N = 8–9) for TNF-α (**C**–**E**) and IL-17 (**H**–**J**). Data are expressed as pg ml^{-1} and presented as Box-and-whisker plots of N = 25 for TNF-α and N = 23 for IL-17 detection. Solid horizontal lines denote the median value ± interquartile ranges (min 25%, max 75%). Statistical analysis was conducted by one-way ANOVA followed by Bonferroni's for multiple comparisons. $^{\#\#\#\#}P \leq 0.0001$ *vs* Ctrl; $^{*}P \leq 0.05$, $^{**}P \leq 0.01$, $^{***}P \leq 0.001$, $^{****}P \leq 0.0001$ *vs* LPS + vehicle.

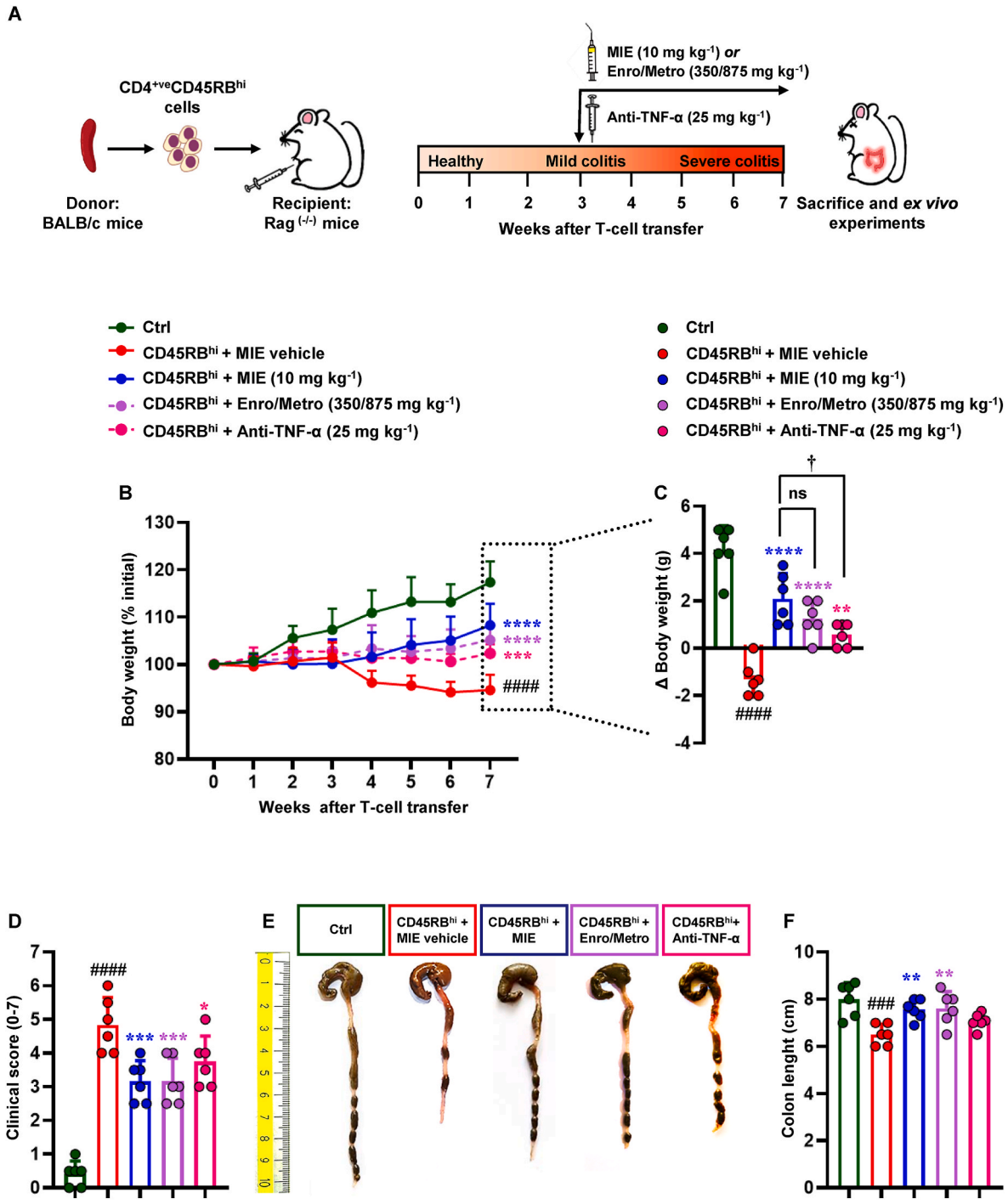

Fig. 2. Therapeutic efficacy of MIE on $CD4^{+}CD45RB^{hi}$ T cells transfer model of colitis. Experimental colitis was induced by the adoptive transfer of $CD4^{+}CD45RB^{hi}$ T cells from healthy donor mice (BALB/c) into RAG1 KO recipient mice. (**A**) Animals were treated therapeutically with MIE (p.o. 10 mg kg^{-1}), anti-TNF-α MAb (i.p. 25 mg kg^{-1}), antibiotic mix Enrofloxacin/Metronidazole (Enro/metro; p.o. 380/875 mg kg^{-1}) or vehicle (150 μl of DMSO/saline 1:3; minimum concentration required to enable solubilization) from week 3, after adoptive transfer, to week 7. Body weight changes (expressed as the percentage of initial body weight) were monitored over time from week 1 to week 7 (**B**), while Δ body weight (expressed as g) was evaluated at the experimental endpoint (week 7) (**C**). Clinical score (assigned from 0 to 7) was observed at week 7 (**D**). Representative photographs of colons isolated from mice were taken (**E**), and colon length in cm was measured at the experimental endpoint (**F**). Data are presented as means ± S.D. of N = 6 mice per group. Statistical analysis was conducted by one- or two-way ANOVA followed by Bonferroni's or Dunnett's for multiple comparisons. $^{\#\#\#}P \leq 0.001$, $^{\#\#\#\#}P \leq 0.0001$ *vs* Ctrl group; $^{*}P \leq 0.05$, $^{**}P \leq 0.01$, $^{***}P \leq 0.001$, $^{****}P \leq 0.0001$ *vs* $CD45RB^{hi}$ + MIE vehicle; $^{\dagger}P \leq 0.05$ *vs* $CD45RB^{hi}$ + MIE 10 mg kg^{-1}.

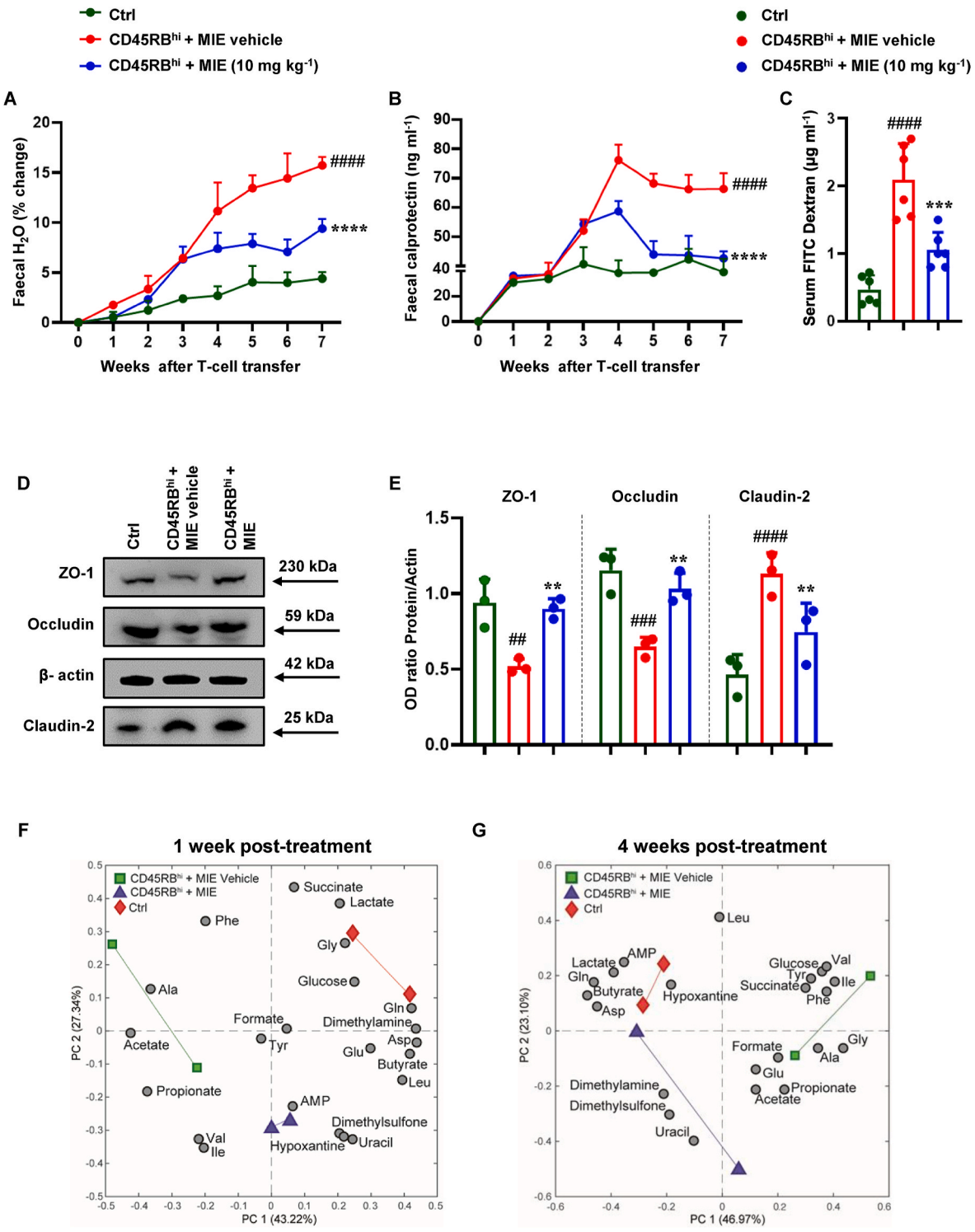

Fig. 3. MIE mitigates excessive gut permeability, tight junction dysregulation and alterations of microbiota-derived metabolites during colitis.
Faecal water contents (expressed as the percentage of water change) (**A**) and faecal calprotectin levels (expressed as ng ml^{-1}) (**B**) from Ctrl, CD45RB^{hi} + MIE vehicle and CD45RB^{hi} + MIE (10 mg kg^{-1}) groups were monitored over time from week 1 to week 7. FITC-4 kDa dextran permeability (expressed as μg ml^{-1}) was evaluated at the experimental endpoint (week 7) (**C**). Thereafter, cell lysates from isolated colonic epithelial cells collected at week 7 were analysed by Western blot for ZO-1 (~230 kDa), occludin (~59 kDa) and claudin-2 (~25 kDa) expression (**D**, **E**). Representative Western blot images are shown from three pooled experiments with similar results (**D**). Cumulative densitometric values are expressed as OD ratio with actin (**E**). Values are presented as means ± S.D. of three separate independent experiments run each with N = 6 mice per group pooled. Statistical analysis was conducted by one- or two-way ANOVA followed by Bonferroni's or Dunnett's for multiple comparisons. $^{\#\#}P \leq 0.01$, $^{\#\#\#}P \leq 0.001$, $^{\#\#\#\#}P \leq 0.0001$ *vs* Ctrl group; $^{**}P \leq 0.01$, $^{***}P \leq 0.001$, $^{****}P \leq 0.0001$ *vs* CD45RB^{hi} + MIE vehicle. PC1 *vs* PC2 biplot of the PCA model was calculated on the metabolome data of faecal samples collected 1 week post-treatment (**F**) and 4 weeks post-treatment (week 7, **G**). Keys: Ile (Isoleucine), Leu (Leucine), Val (Valine), Ala (Alanine), Glu (Glutamate), Gln (Glutamine), Asp (Aspartate), Tyr (Tyrosine), Gly (Glycine), Phe (Phenylalanine).

3. Results and discussion

3.1. Beneficial impact of MIE in LPS-stimulated blood taken from UC, IBS, and CD patients

Current conventional treatments for IBD are aimed at controlling inflammation by administering anti-inflammatory agents, including steroids, immunosuppressive drugs, and biological agents targeting inflammatory cytokines (mainly TNF-α and IL-17) for refractory and severe forms of IBDs [75,76]. However, approximately one-third of patients receiving anti-TNF-α agents do not respond to treatment (primary failure), and a significant proportion (up to 50%) become refractory over time (secondary failure) [77]. Intestinal barrier dysregulation leads to systemic release of bacterial components (e.g., LPS) into circulation, leading to an acute inflammatory response. To model this, we spiked patient blood with LPS (as a tool to induce a controlled immune response and investigate specific aspects of inflammatory pathways) and assessed the impact of MIE on TNF-α and IL-17 production (Patients information in Table 1). LPS induced an increase in TNF-α and, in part, IL-17 secretion within the sera from IBS, UC and CD (Fig. 1). MIE caused a dose-dependent reduction in TNF-α following LPS in all patient groups (Fig. 1A-**E**) and healthy donors (Supplementary Fig. 7). By contrast, MIE caused a dose-dependent reduction in IL-17 concentrations in LPS-spiked serum from IBS and CD patients, but not UC, with significant reductions only seen at the highest concentration of MIE (Fig. 1F-**J**). Low numbers within the individual patient groups mean it is difficult to make definitive conclusions about whether MIE might be therapeutically beneficial in specific disease groups. Moreover, the limitation in the amount of blood available has restricted our ability to recover sufficient sera for a comprehensive analysis of multiple analytes. Despite these limitations, these data indicate that MIE has the potential to effectively alleviate pathological pro-inflammatory responses in IBD patients suffering intestinal barrier dysregulation, with some disease-specific benefits. On these premises, we have designed an experimental approach to understand the possible mechanism of action involved.

3.2. MIE extract ameliorates the development of $CD4^{+}CD45RB^{hi}$ T cell-induced colitis

We have recently shown that a *Mangifera indica* L. extract (MIE) at 90% purity in mangiferin was able to modulate COX-2/mPGES-1 axis, and Th17/Treg repertoire in a well-established *in vivo* model of gouty arthritis [20], paradigmatic of local, but also systemic, inflammation [47,49]. In a previous paper, we demonstrated, through a pharmacokinetic study, that MIE given orally displays a similar plasma concentration and *in vivo* toxicological profile to the pure compound mangiferin [20]. However, *in vitro* cytotoxic examination revealed a safer profile for MIE compared to the pure compound on murine macrophage cell lines [20]. To provide a mechanistic insight, we assessed the efficacy of the extract in a T cell-driven model of colitis in a therapeutic fashion i.e. once the disease is established (Fig. 2A and Supplementary Fig. 1). As previously reported [21,29], RAG1 KO mice receiving WT $CD4^{+}CD45RB^{hi}$ cells (Fig. 2A) develop symptoms of colitis, including significant weight loss by week 4 post transfer (Fig. 2B), reaching the maximum clinical score at week 7 (Fig. 2C). In contrast, the administration of MIE (10 mg kg^{-1}) from week 3 (Fig. 2A), in a therapeutic fashion, ameliorated weight loss (Fig. 2B and **C**), clinical score (including mice hunching and wasting, colon thickening or inflammation, and stool consistency) (Fig. 2D) and colon shortening/length (Fig. 2E and **F**). No significant effects were revealed macroscopically for small intestine length (Supplementary Fig. 8). Importantly, the effects of MIE were comparable to RAG1 KO mice receiving current standard of care (anti-TNF-α) or antibiotic treatment (Enro/Metro) (Fig. 2B-**F**). These data demonstrate that MIE displays a potent anti-inflammatory/protective activity as compared to that observed with biological and antibiotic therapies commonly utilised for IBDs treatment, in both preclinical and clinical protocols [36].

3.3. MIE counteracts mucosal inflammation, damage to epithelial integrity and alterations of microbiota-derived metabolites in favour of an immunoregulatory phenotype

Increased colitis and mucosal inflammation cause paracellular permeability and damage to epithelial integrity [78]. This is associated with disruption of tight junction proteins, such as claudins and occludins, an increase of H_2O faecal content [79], and leukocyte accumulation in the stool due to the release of calprotectin (heterodimeric S100A8/S100A9 complex) [80]. Roseth AG et al. were the first to demonstrate an increase in faecal calprotectin concentrations in patients with IBD [81]. Currently, this marker is a routine clinical assessment tool to distinguish IBD from IBS, with an elevated sensitivity and specificity in the adult population [78]. As expected, the $CD4^{+}CD45RB^{hi}$ vehicle-treated group revealed the highest concentration of faecal H_2O and calprotectin in the stools (Fig. 3A and **B**), whereas MIE significantly reduced the concentration of these markers almost back to baseline levels (Fig. 3A and **B**). Subsequently, to verify the integrity of intercellular junctional complexes, we assessed intestinal leakage of FITC dextran and expression of ZO-1, occludin and claudin-2 proteins. Induction of colitis results in a significant increase in serum FITC dextran when compared to untreated animals, consistent with damaged barrier function (Fig. 3C). Importantly, these effects were largely absent in MIE-treated animals (Fig. 3C). Supporting these observations, epithelial junctional proteins, ZO-1 and occludin, were significantly reduced in mice with colitis compared to untreated, non-inflamed animals, whereas MIE-treated group restored these to physiological levels (Fig. 3D and **E**). Conversely, claudin-2 expression was elevated in response to intestinal inflammation, and this was reversed upon therapeutic administration of MIE (Fig. 3D and **E**). Thus, MIE can restore the apical junction complex, ensuring balanced permeability of the intestinal barrier and protection against diarrhoea and rectal bleeding observed in colitis [82].

Characterisation of the host-microbiota is crucial in the context of intestinal disorders, such as IBDs, in which the gut environment is severely perturbed, yet the disease-causing mechanisms are still largely unknown. Reductions of gut barrier-protecting short-chain fatty acids (SCFA) and alterations in bile acids, sphingolipids and tryptophan-derived metabolites have been consistently reported in faeces of patients with IBD [83,84]. Considering that a subset of small molecules, including microbiome-derived metabolites, have been shown to regulate the immune response, it is crucial to characterise these metabolites and understand which factors determine their concentrations in the gut. In this context, the characterisation of faecal metabolites holds great potential for discovering non-invasive biomarkers and therapeutic targets. Firstly, we characterized, metabolites in faecal stools collected throughout the experiment (Supplementary Fig. 9A). Microbiota-derived metabolites (e.g. lactate, succinate), products from alteration of microflora population (e.g. uracil, hypoxanthine) and products from dysbiosis (e.g. propionate, butyrate and acetate) [84], were unbalanced as early as 1 week post onset of colitis compared to untreated/non-inflamed animals and are further dysregulated as the disease progresses over the 7 weeks (Supplementary Figs. 9B–H).

Among different gut-microbiota-derived metabolites, the most well-characterized are the end products of dietary fibre fermentation and the SCFAs. Of note, MIE treatment was able to reverse the metabolic imbalance as early as 1 week post-treatment (week 4, Fig. 3F), with a transitional metabolite phenotype seen at 4 weeks post-treatment (week 7, Fig. 3G), although not quite back to baseline/untreated profiles. This metabolic shape and change may serve as an important source of nutrients for intestinal epithelial cells, supporting barrier function and may act as important cellular mediators regulating gene expression, cell differentiation, and gut tissue development [85]. We did not specifically investigate the direct effects of *Mangifera indica* extract on microbiota

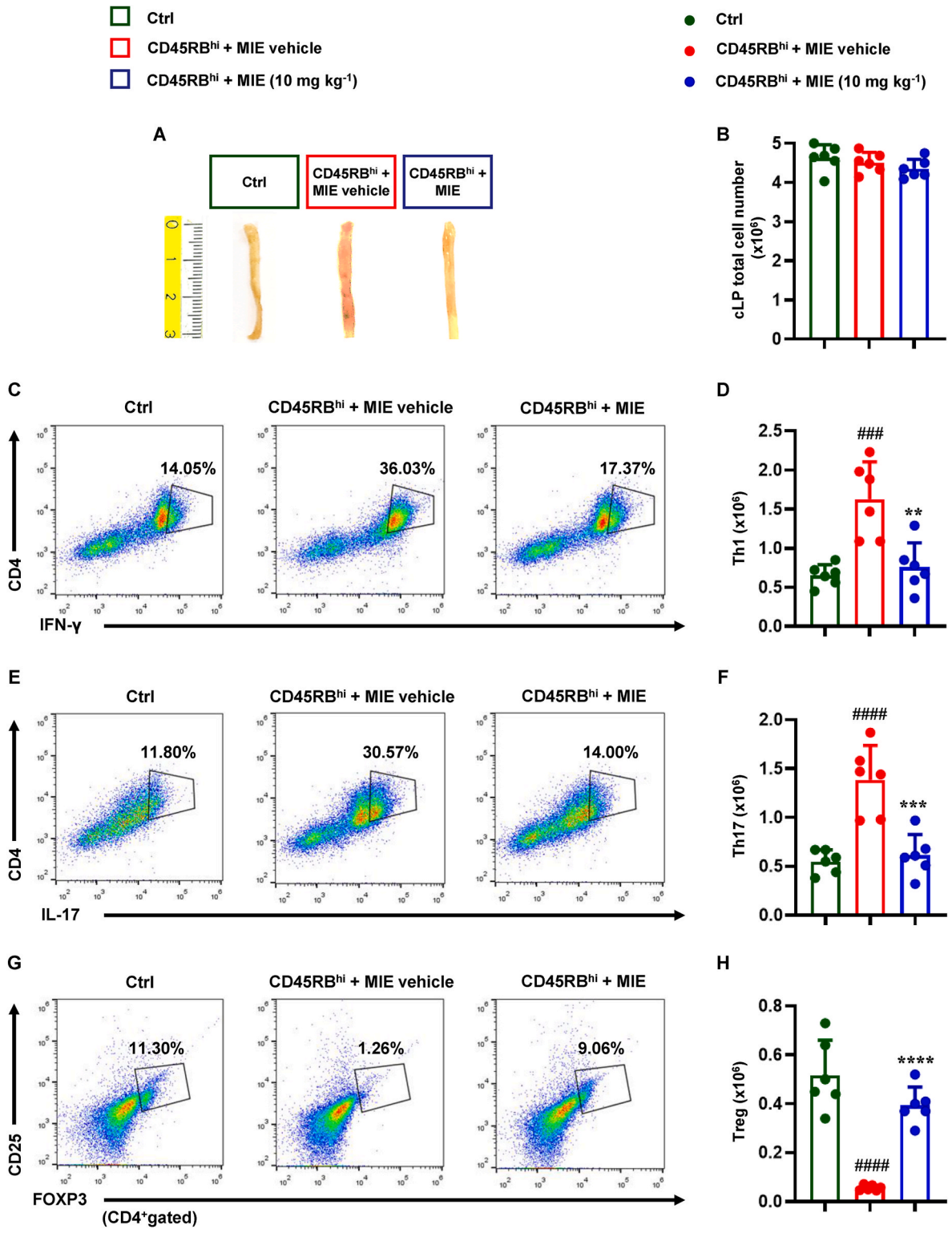

Fig. 4. MIE modulates Th1/Th17 and Treg cell expansion in the colonic lamina propria.
At the experimental endpoint (week 7), colon samples from Ctrl, CD45RB^{hi} + MIE vehicle and CD45RB^{hi} + MIE (10 mg kg^{-1}) groups were dissected and analysed macroscopically. Representative photographs of colon sections from the different experimental conditions are shown in (**A**). Subsequently, flow cytometry analysis was employed to determine Th1, Th17 and Treg lymphocyte subsets. For this purpose, colons were digested, and isolated cLP cells were counted (**B**) and gated in their totality and singlet (see flow cytometry strategy reported in Supplementary Fig. 2) before the identification of CD4$^+$IFN-γ$^+$ (**C**, **D**, Th1 population), CD4$^+$IL-17$^+$ (**E**, **F**, Th17 population) and CD4$^+$CD25$^+$FOXP3$^+$ (**G**, **H**, Treg population). FACS pictures are presented as dot plot (pseudocolor), whereas % of positive cells are reported on the respective gates. Histograms indicate the total positive populations (expressed as x10^6 and calculated from means of % of positive cells) in the different experimental conditions (**D**, **F**, **H**). Data are presented as means ± S.D. of N = 6 mice per group. Statistical analysis was conducted by one-way ANOVA followed by Bonferroni's for multiple comparisons: $^{###}P \leq 0.001$, $^{####}P \leq 0.0001$ *vs* Ctrl group; $^{**}P \leq 0.01$, $^{***}P \leq 0.001$, $^{****}P \leq 0.0001$ *vs* CD45RB^{hi} + MIE vehicle.

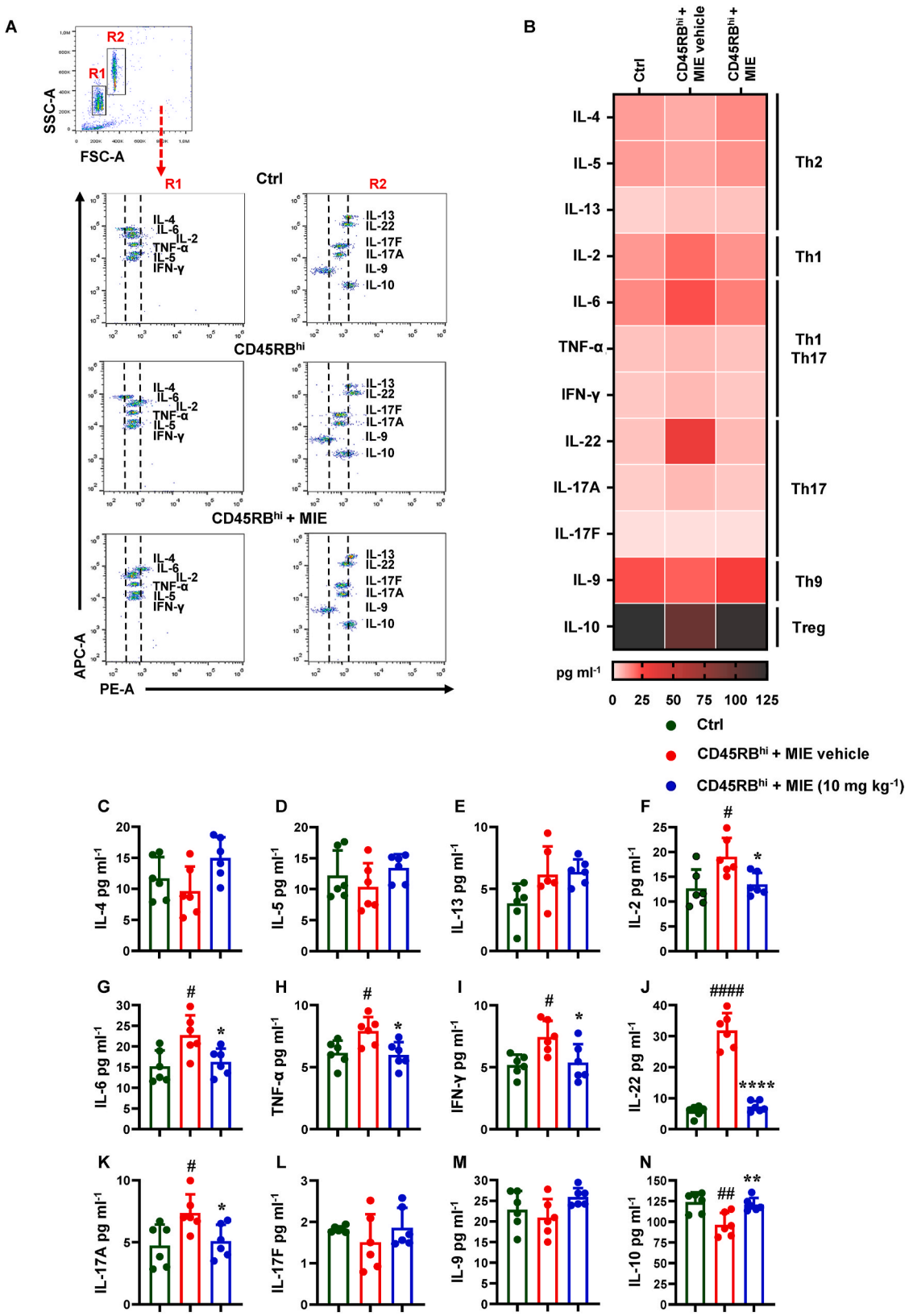

Fig. 5. MIE affects the release of colonic Th-related cytokines. Supernatants of colon tissue homogenates from Ctrl, CD45RB^{hi} + MIE vehicle and CD45RB^{hi} + MIE (10 mg kg^{-1}) at the experimental endpoint (week 7) were assayed using a multi-LEGENDplex™ analyte flow array (**A**). Quantification of Th-related cytokines is presented as a heatmap and expressed as pg ml^{-1} (**B**). Thereafter, all pro- and anti-inflammatory cytokines were extrapolated from the heatmap and represented graphically as histograms (pg ml^{-1}): IL-4 (**C**), IL-5 (**D**), IL-13 (**E**), IL-2 (**F**), IL-6 (**G**), TNF-α (**H**), IFN-γ (**I**), IL-22 (**J**), IL-17A (**K**), IL-17F (**L**), IL-9 (**M**) and IL-10 (**N**). Data are presented as means ± S.D. of N = 6 mice per group. Statistical analysis was conducted by one-way ANOVA followed by Bonferroni's for multiple comparisons. $^{\#}P \leq 0.05$, $^{\#\#}P \leq 0.01$, $^{\#\#\#\#}P \leq 0.0001$ *vs* Ctrl group; $^{*}P \leq 0.05$, $^{**}P \leq 0.01$, $^{****}P \leq 0.0001$ *vs* CD45RB^{hi} + MIE vehicle.

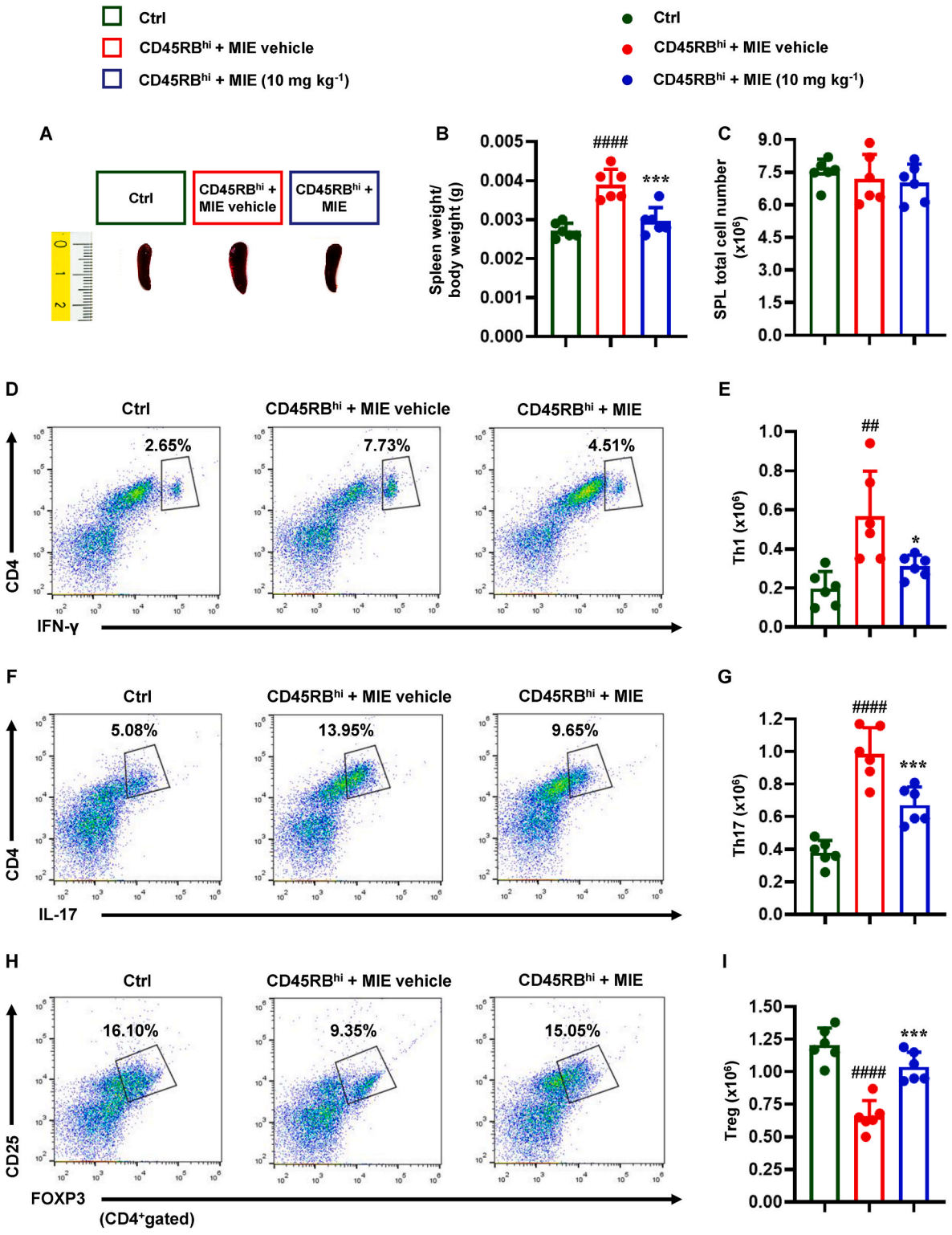

Fig. 6. The immunomodulatory property of MIE is mirrored in splenic Th1/Th17 and Treg cell repertoire.
At the experimental endpoint (week 7), spleen samples from Ctrl, CD45RB^{hi} + MIE vehicle and CD45RB^{hi} + MIE (10 mg kg^{-1}) groups were dissected and analysed macroscopically. Representative photographs are shown in (**A**), and the spleen weight/mouse body weight ratio was evaluated (**B**). Subsequently, flow cytometry analysis was employed to determine splenic Th1, Th17 and Treg lymphocyte subsets. For this purpose, spleens were smashed, tested for total cell count (**C**), and gated in their totality and singlet (see flow cytometry strategy reported in Supplementary Fig. 3) before the identification of CD4$^+$IFN-γ$^+$ (**D**, **E**, Th1 population), CD4$^+$IL-17$^+$ (**F**, **G**, Th17 population) and CD4$^+$CD25$^+$FOXP3$^+$ (**H**, **I**, Treg population). FACS pictures are presented as dot plot (pseudocolor), whereas % of positive cells are reported on the respective gates. Histograms indicate the total positive populations (expressed as x10^6 and calculated from means of % of positive cells) in the different experimental conditions (**E**, **G**, **I**). Data are presented as means ± S.D. of N = 6 mice per group. Statistical analysis was conducted by one-way ANOVA followed by Bonferroni's for multiple comparisons. $^{\#\#}P \leq 0.01$, $^{\#\#\#\#}P \leq 0.0001$ *vs* Ctrl group; $^*P \leq 0.05$, $^{***}P \leq 0.001$ *vs* CD45RB^{hi} + MIE vehicle.

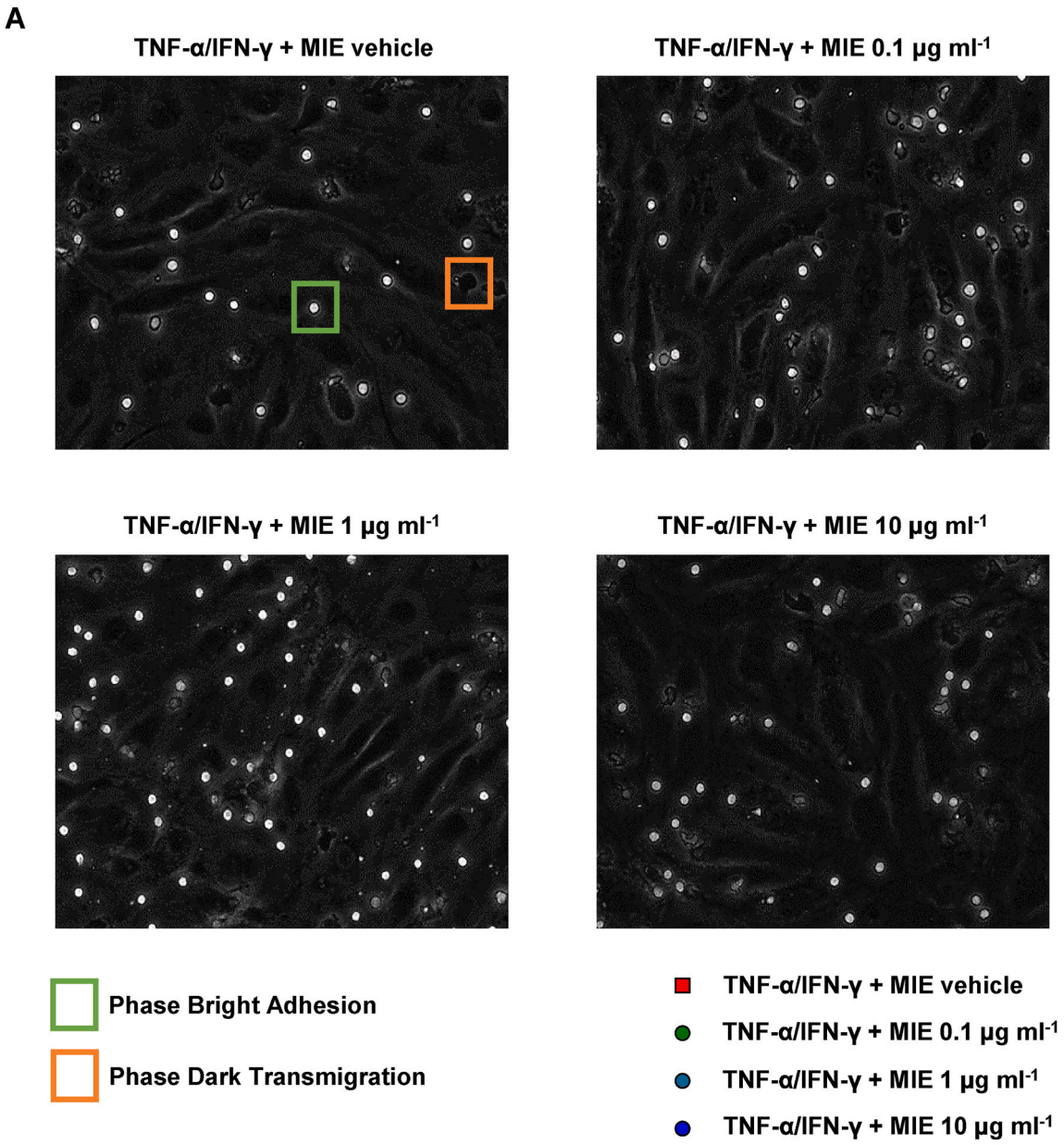

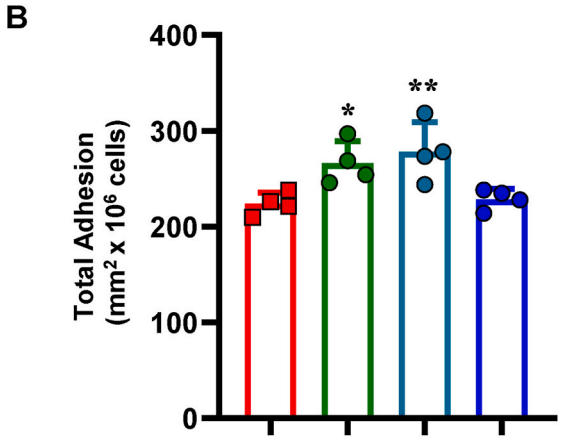

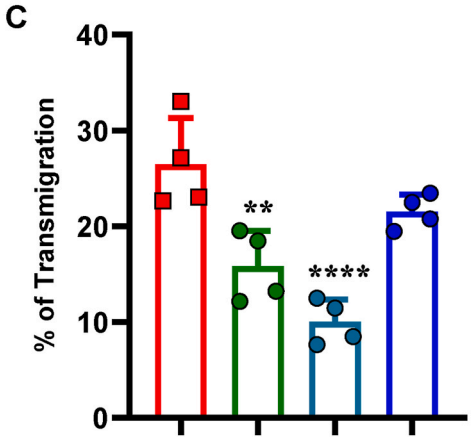

(caption on next page)

Fig. 7. Effect of MIE on PBLs static adhesion/migration assay.
In a static adhesion/migration assay, HDBECs were treated with TNF-α (100 U ml^{-1}) and IFN-γ (10 ng ml^{-1}) in presence of MIE extract (0.1–10 μg ml^{-1}) or its corresponding vehicle (DMSO, 0.25%) for 24 h. PBLs were added for 7 min on stimulated HDBEC, followed by washing to remove all non-adherent cells. In the panel **A** representative images of PBLs adhesion (indicated as phase bright and spherical in morphology, green square) and transmigration (indicated as black and elongated morphology, orange square) are shown. Quantification of PBLs total adhesion (expressed as mm^2 x 10^6 cells) (**B**) and % of transmigration (**C**) was performed using Image-pro 7.0 software. Data are presented as means ± S.D. of N = 4 independent healthy donors. Statistical analysis was conducted by one-way ANOVA followed by Bonferroni's for multiple comparisons. *P ≤ 0.05, **P ≤ 0.01, ****P ≤ 0.0001 *vs* TNF-α/IFN-γ + MIE vehicle.

composition in this study. To address this important aspect, we plan to incorporate microbiota analyses in our future investigations.

3.4. The immunomodulatory activity of MIE on the progression of colitis

To dissect the anti-inflammatory and immunomodulatory activity of MIE, we next evaluated the ability of MIE to modulate the T cell immune cell infiltrate [21,86,87]. Isolated colonic lamina propria (week 7) (Fig. 4A) was digested and infiltrated cells isolated (Fig. 4B) were phenotyped by flow cytometry, as previously described [43,44]. Colitis significantly increased Th1 (Fig. 4C and **D**) and Th17 populations (Fig. 4E and **F**), with a concomitant decrease of Treg cells when compared to untreated/non-inflamed animals (Fig. 4G and **H**). Importantly, MIE reversed these changes, reducing the frequency of pathogenic Th1 and Th17 cells and increasing protective Tregs within the intestine (Fig. 4C-**H**). Our results indicate that MIE controls the induction and progression of gut inflammation by restoring the immunological imbalance associated with this disease.

We next analysed whether the levels of intestinal pro/anti-inflammatory cytokines were modulated after MIE treatment (Fig. 5A and **B**), as previously described [59]. We observed a significant increase in cytokines associated with a Th1 and Th17 profile in colitis animals compared to untreated controls (Fig. 5B-N). Of particular interest, administration of MIE significantly down-regulated IL-2 (Fig. 5B and **F**), IL-6 (Fig. 5B and **G**), TNF-α (Fig. 5B and **H**), IFN-γ (Fig. 5B and I), IL-22 (Fig. 5B and **J**), IL-17A (Fig. 5B and **K**) and concomitantly increased IL-10 levels compared to vehicle control group (Fig. 5B and **N**). These data suggest that MIE inhibits the induction of pathogenic T-cells and their associated cytokines, leading to the reduced disease severity observed in this model.

An immunologically important, yet undefined aspect of disease pathogenesis in animal models of IBD, is the anatomic location(s) where naïve T cells encounter enteric antigens to yield colitogenic effector cells. It has been assumed that naïve T cells migrate to the gut-associated lymphoid tissue (e.g. GALT and Peyer's patches), as well as the spleen. In this environment, T cells play important roles in mounting mucosal immune responses to invading pathogenic and/or commensal microorganisms to minimize the tissue inflammation and systemic immune activation that may arise from these protective responses [88,89]. In our preclinical assessment, mice with colitis displayed splenomegaly (Fig. 6A and **B**) with no significant difference in terms of total cell number (Fig. 6C). This increase was mirrored by an expansion of both infiltrated Th1 (Fig. 6D and **E)** and Th17 cells (Fig. 6F and **G**) and a concomitant reduction of Treg repertoire within the spleen (Fig. 6H and I) in animals with colitis compared to controls. Importantly, treatment with MIE prevented splenomegaly (Fig. 6A and **B**) and dysregulation of T-cell trafficking (Fig. 6D-**I**). Collectively, these data highlight the systemic effects of MIE in modulating lymphocyte trafficking between intestinal and secondary lymphoid tissues to mitigate intestinal inflammation and disease progression.

3.5. MIE inhibits lymphocyte trafficking across endothelial cells via DP2 prostanoid receptor

Effector memory lymphocytes enter tissue via blood vascular endothelial cells (BVEC) and leave tissue via lymphatic vascular endothelial cells (LVEC). During inflammation, memory T cells are recruited to tissue after capture by specialized, fast-acting adhesion receptors (i.e., VCAM-1 and E− or P-selectin) on up-regulated BVEC in response to inflammatory stimuli [90]. To assess whether MIE directly influences lymphocyte trafficking, we analysed the effects of increasing MIE concentrations on lymphocyte adhesion and transendothelial migration across inflamed BVEC (Fig. 7A). MIE displayed a bell-shaped response within the dose frame studied. Up to a dose of 1 μg ml^{-1} significantly increased lymphocyte adhesion, with a concomitant reduction in transendothelial migration (Fig. 7A-**C**) when compared to vehicle control. In addition, T cells egress from the site of inflammation is necessary for immune surveillance and the efficient regulation and resolution of the immune response [91,92]. Current paradigms of T cell trafficking during an inflammatory response assume that the delivery of a chemokine signal is sufficient to promote integrin-mediated stable adhesion, followed by reorganization of the actin cytoskeleton during spreading on the endothelial cells (EC) surface, eventually leading to transendothelial migration. However, recent evidence demonstrates that blockade of the prostanoid PGD_2 receptor DP2 at the vascular level [formally known as chemoattractant receptor-homologous molecule expressed on Th2 cells (CRTh2)] greatly reduces the transmigration of memory T cells, leaving the great majority attached to the apical surface of the EC monolayer [63]. This allows us to speculate that although an initial chemokine signal is essential for activating T cells on EC, a downstream prostanoid signal, delivered by PGD_2 via the DP2 receptor, is required to drive the process of diapedesis. In order to provide a more detailed characterization of the adhesion response in the context of IBD, our future studies will follow up with patients who have received a confirmed diagnosis of UC or CD, isolating CD4 T cells and conducting more targeted and informative adhesion experiments.

We next investigated whether the upstream prostaglandin signal was modulated in response to MIE treatment. Arachidonic acid metabolism through COX enzymes (1 and 2) leads to the generation of PGH_2, which is further metabolised into PGD_2 and PGE_2 through specific prostaglandin synthetases. Three PGES isoenzymes have been characterized to date, two microsomal isoforms (mPGES-1 and mPGES-2) and one cytosolic isoform (cPGES) [93]. The inducible PGES (mPGES-1) seem to be the essential PGES isoenzyme involved in PGE_2 biosynthesis by human vascular cells [94,95]. Both PGD_2 and PGE_2 can signal through the DP receptors, with DP2 specifically expressed on T-cells. In response to TNF-α and IFN-γ, BVEC up-regulates COX-2 and DP2 expression, whilst DP1 remains unchanged (Fig. 8A and **B**). In line with the literature, mPGES1 was not expressed [96]. As anticipated, enhanced COX-2 expression resulted in increased PGE_2 and PGD_2 secretion from inflamed BVEC (Fig. 8C and **D**). This agrees with several previous publications [97], although others have been unable to detect PGE2 production in human umbilical vein-derived endothelial cells (HUVEC) [94]. Interestingly, MIE was able to reverse this inflammation-induced change in COX-2 and DP2 (Fig. 8A and **B**), leading to reduced PGE_2 and PGD_2 secretion (Fig. 8C and **D**). Similar findings were observed in the inflamed colon, whereby colitis significantly increased expression of COX-2, mPGES-1, DP2, PGD_2, and PGE_2 and this was reduced back to baseline levels by therapeutic administration of MIE (Fig. 8E-**H**). These data are in agreement with previous reports which reveal that PGD_2 is required for T cell trafficking via the DP2 receptor [63] and demonstrate that MIE can directly regulate this expression.

Given the biological activity herein described obtained with mangiferin extract, we finally postulated a possible direct interaction between mangiferin and the DP2 receptor. To gain a better understanding of how mangiferin may bind to DP2 receptor at an atomic level,

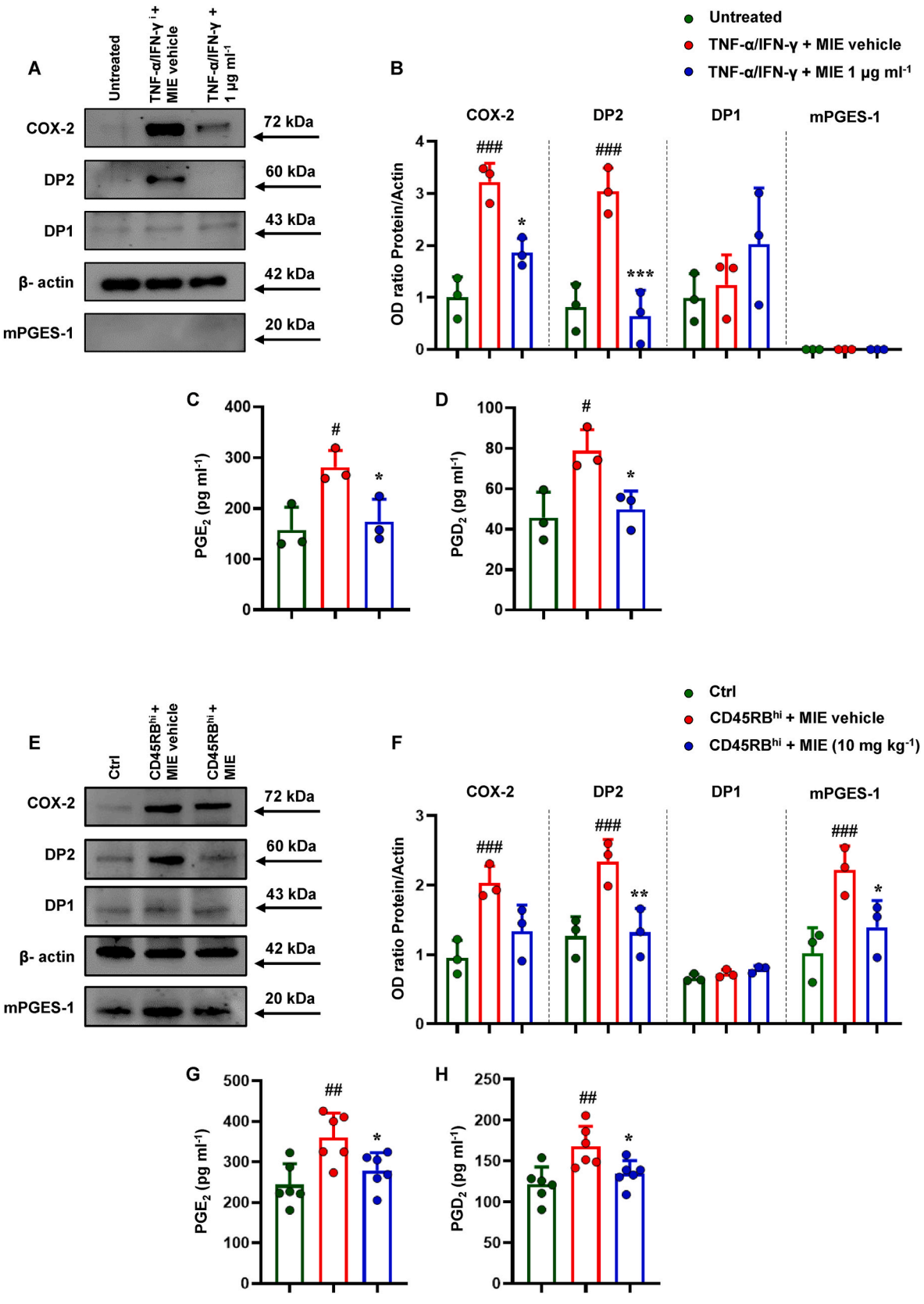

(caption on next page)

Fig. 8. MIE acts as a regulator of the PGD_2/DP2 prostanoid receptor axis.
HDBECs were treated with TNF-α (100 U ml^{-1}) and IFN-γ (10 ng ml^{-1}) in presence of MIE extract (1 μg ml^{-1}) or its corresponding vehicle (DMSO, 0.25%) for 24 h. Cell pellet lysates from all experimental conditions were assayed by Western blot for COX-2 (~72 kDa), DP2 (~60 kDa), DP1(~43 kDa) and mPGES-1(~20 kDa) expression (**A**, **B**), whereas supernatants were assayed by ELISA for PGE_2 (**C**) and PGD_2 (**D**) levels (pg ml^{-1}). Representative Western blot images are shown from three independent experiments with similar results (**A**). Cumulative densitometric values (**B**) are expressed as OD ratio with actin. Values are presented as means ± S.D. of 3 independent experiments. Statistical analysis was conducted by one-way ANOVA followed by Bonferroni's for multiple comparisons. $^{\#}P < 0.05$, $^{\#\#\#}P < 0.001$ *vs* untreated group; $^{*}P < 0.05$, $^{***}P < 0.001$ *vs* TNF-α/IFN-γ + MIE vehicle. Colon tissue homogenates from $CD4^{+}CD45RB^{hi}$ T cells transfer model were assayed by Western blot for all afore-mentioned biomarkers (COX-2, DP2, DP1 and mPGES-1; **E**, **F**) and by ELISA for PGE_2 (**G**) and PGD_2 (**H**) levels (pg ml^{-1}). Representative Western blot images are shown from three independent experiments with similar results (**E**). Cumulative densitometric values (**F**) are expressed as OD ratio with actin. Values are presented as means ± S.D. of three separate independent experiments run each with N = 6 mice per group pooled. Statistical analysis was conducted by one-way ANOVA followed by Bonferroni's for multiple comparisons. $^{\#\#}P \leq 0.01$, $^{\#\#\#}P < 0.001$ *vs* Ctrl group; $^{*}P \leq 0.05$, $^{**}P \leq 0.01$ *vs* $CD45RB^{hi}$ + MIE vehicle.

molecular docking studies were performed using the DP2 X-ray structure (PDB code: 6D27), co-crystalized with the potent and selective antagonist fevipiprant [98]. This compound, as well as other recently discovered selective DP2 antagonists, like ramatroban [99], is a nonlipid PGD_2 analogue possessing a polycyclic aromatic central scaffold and a carboxylic function. Docking calculations of mangiferin to the DP2 receptor were performed with the aid of Glide within the Schrodinger package (see Methods section for details). Results converge on a set of poses very similar to one another, all concentrated in the middle of the receptor binding pocket with the same orientation. Specifically, in the majority of the found poses mangiferin was superimposable with the co-crystallized fevipiprant (Supplementary Figs. 10A and B). Specifically (see Supplementary Fig. 10A), the central aromatic core of mangiferin forms a parallel π-π with the Y183 side chain and engages in extensive aromatic and hydrophobic interactions with F90, L286, F87, H95 and W283 side chains. Interestingly, the hydroxyl group in position 1 forms an H-bond with the main chain amine group of C182. The sugar moiety of mangiferin plunges toward the bottom of the pocket, surrounded by the F87, F111, F112, and F294 residues, and is involved in multiple H-bonds with the R170, Y184, H107 and Y262 side chains. All these interactions are also formed by fevipiprant. Of note, the above-described interaction network of mangiferin within the DP2 receptor, suggests an antagonist potential of this molecule toward the receptor, in line with our biological data, although a direct binding assay would certainly be required to validate this model [100].

4. Conclusion

Here starting from the current literature evidence and by the finding that *Mangifera indica* L. displays a beneficial effect in IBD patient blood samples we have defined a mechanism of action which targets the prostanoid pathway. This modulation directly impacts on lymphocyte trafficking via DP2 receptor (Fig. 9). Thus, the use of mangiferin or its derivatives in the treatment of IBD could represent an efficacious add-on to current therapeutic interventions biologic, also due to its tolerability profile. Furthermore, our findings strengthen the rationale for a clinical trial/s to assess the efficacy in humans and individuates the measurement of PGE_2 and PGD_2 in blood as surrogate non invasive markers to be used in association/correlation with the typical clinical endpoints used in IBD studies.

Declaration of competing interest

This article has been conducted and written in the absence of any commercial or financial relationships that could be construed as a potential conflict of interest.

Data, materials and software availability

All data associated with this study are present in the paper or the Supplementary Data. Request for reagents should be directed to the corresponding authors and will be made available after completion of a material transfer agreement with the University of Naples.

Funding and acknowledgements

This research has been in part supported by The National Institute of Health and Care Research (NIHR) Birmingham Biomedical Research Centre (NIHR203326). This work was also supported by a Medical Research Council project grant MR/T028025/1. A.Sa. is supported by Dompé farmaceutici S.p.A fellowship for PhD program in "Nutraceuticals, functional foods and human health" (University of Naples Federico II), whereas A.Sc. is supported by University of Naples Federico II PhD scholarship in "Nutraceuticals, functional foods and human health" (PNRR DM 118 M4C1– INV 4.1 ricerca PNRR generici). I.B is supported by University of Naples Federico II PhD scholarship in "Nutraceuticals, functional foods and human health", whereas M.S. is supported by the University of Naples Federico II PhD scholarship in Pharmaceutical Sciences. A.J.I. was supported by Birmingham Fellowship. A.A.M. was supported by a King Khalid University funded PhD Scholarship (57875). The opinions expressed in this paper are those of the authors and do not represent any of the listed organisations. The authors would like to thank L.C.M. Trading S.p.A. (Italy) for excellent technical assistance and scientific discussions on the manuscript. The views expressed in this publication are those of the author(s) and not necessarily those of the L. C.M. Trading S.p.A. and Dompé farmaceutici S.p.A.

CRediT authorship contribution statement

Anella Saviano: Conceptualization, Data curation, Formal analysis, Investigation, Methodology, Visualization, Writing – original draft. **Anna Schettino:** Conceptualization, Data curation, Formal analysis, Investigation, Methodology, Visualization. **Nunzia Iaccarino:** Data curation, Investigation, Methodology, Visualization. **Adel Abo Mansour:** Data curation, Investigation. **Jenefa Begum:** Data curation, Investigation. **Noemi Marigliano:** Data curation, Investigation. **Federica Raucci:** Data curation, Investigation. **Francesca Romano:** Data curation, Investigation. **Gelsomina Riccardi:** Data curation, Investigation. **Emma Mitidieri:** Data curation, Investigation. **Roberta d'Emmanuele di Villa Bianca:** Data curation, Investigation. **Ivana Bello:** Data curation, Investigation. **Elisabetta Panza:** Data curation, Investigation. **Martina Smimmo:** Data curation, Investigation. **Valentina Vellecco:** Data curation, Investigation. **Peter Rimmer:** Data curation, Investigation. **Jonathan Cheesbrough:** Data curation, Investigation. **Zhaogong Zhi:** Data curation, Investigation. **Tariq H. Iqbal:** Data curation, Investigation. **Stefano Pieretti:** Data curation, Investigation. **Vincenzo Maria D'Amore:** Data curation, Investigation. **Luciana Marinelli:** Data curation, Investigation. **Valeria La Pietra:** Data curation, Investigation, Visualization, Writing – original draft. **Raffaella Sorrentino:** Investigation. **Luisa Costa:** Investigation. **Francesco Caso:** Investigation. **Raffaele Scarpa:** Data curation. **Giuseppe Cirino:** Writing – original draft. **Antonio Randazzo:** Writing – original draft. **Mariarosaria Bucci:** Writing – original draft. **Helen Michelle McGettrick:** Investigation, Writing – original draft, Writing – review & editing. **Asif Jilani Iqbal:** Conceptualization, Formal analysis, Investigation, Project administration, Writing – original draft, Writing – review & editing. **Francesco Maione:** Conceptualization, Formal analysis, Investigation, Project administration, Supervision, Writing – original

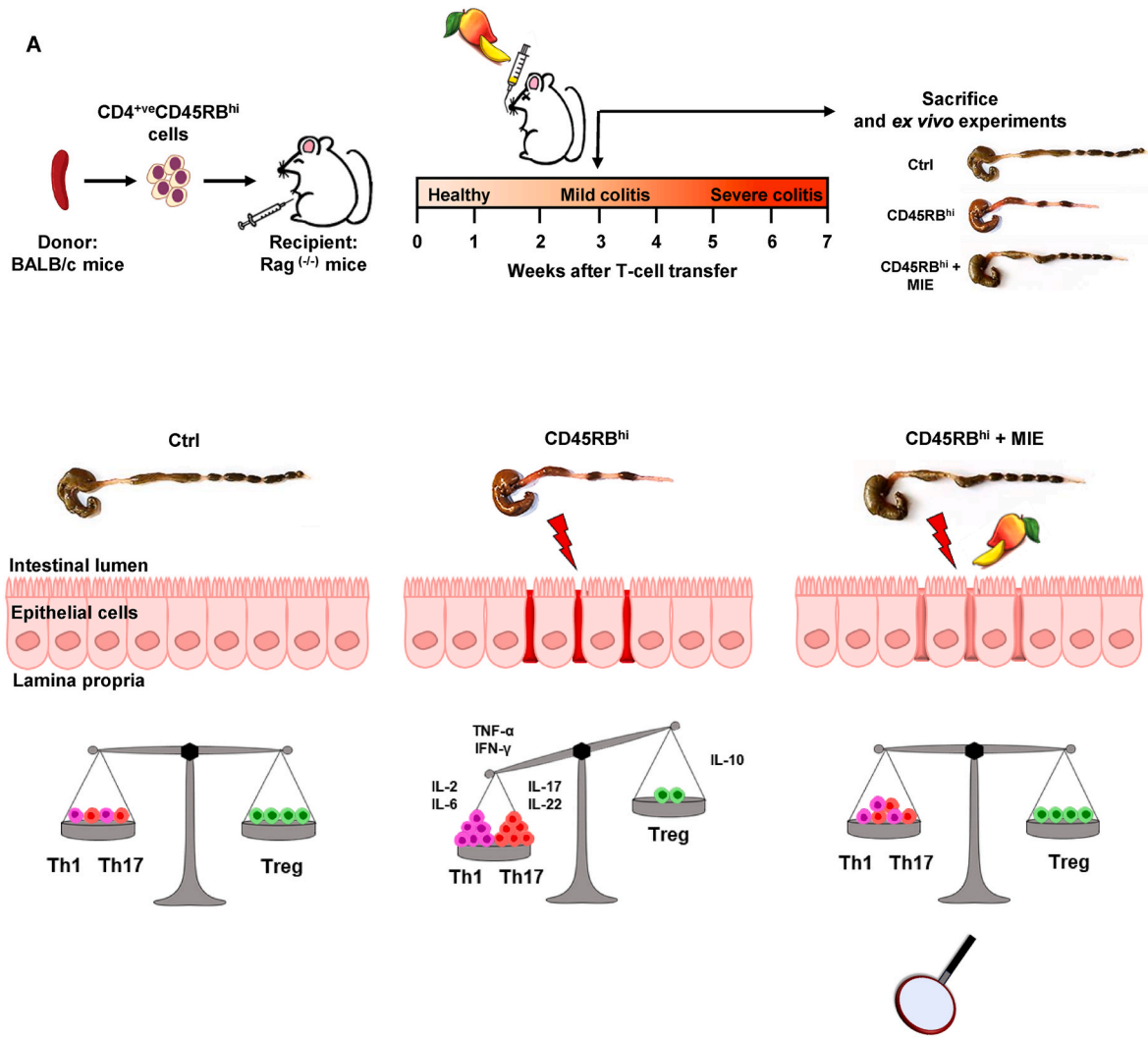

Fig. 9. A model of the proposed mechanism by which MIE exerts anti-inflammatory and immunomodulatory activity against colitis.
MIE ameliorates intestinal inflammation and immunological perturbance induced by $CD4^{+}CD45RB^{hi}$ T cell transfer by regulating Th1/Th17 cells' egress and restoration of Treg balance on colonic lamina propria (**A**). Specifically, an overview of the steps in the regulation of T cell trafficking by which MIE act via the PGD_2/DP2 prostanoid receptor axis to mediate its immunomodulatory effects (**B**). Step 1: Endothelial cells (EC) stimulated with cytokines (TNF-α and IFN-γ) selectively recruit $CD4^{+}$ lymphocytes from flowing blood. Step 2: The T cells receive an activating stimulus from IFN-γ–inducible chemokines on the chemokine receptor CXCR3. Step 3: T cell integrins are transiently activated and immobilize the cell on the surface of activated EC. Prostaglandin D_2 (PGD_2), generated by the action of cyclooxygenase enzyme (COX-2) on the arachidonic acid (AA), binds the PGD_2 receptor DP2. Step 4: DP2 generates signals that stabilise lymphocyte adhesion, induce lymphocytes to shape change, and support the process of transmigration across the endothelial cell monolayer. If the endothelial cells have been supplemented with MIE, it modulates PGD_2/DP2-mediated PBLs responses, reducing massively lymphocyte adhesion and migration across EC.

draft, Writing – review & editing.

Data availability

Data will be made available on request.

Appendix A. Supplementary data

Supplementary data to this article can be found online at https://doi.org/10.1016/j.jaut.2024.103181.

References

[1] F. Carbonnel, M.C. Boutron, Incidence, phenotype, and Mortality of inflammatory bowel disease 'twenty years after, J Crohns Colitis 11 (2017) 1159–1160.
[2] E. Bequet, H. Sarter, M. Fumery, F. Vasseur, L. Armengol-Debeir, B. Pariente, et al., Incidence and phenotype at diagnosis of very-early-onset compared with later-onset paediatric inflammatory bowel disease: a population-based study [1988-2011], J Crohns Colitis 11 (2017) 519–526.
[3] P. Yadav, D. Ellinghaus, G. Rémy, S. Freitag-Wolf, A. Cesaro, F. Degenhardt, et al., Genetic factors interact with tobacco smoke to modify risk for inflammatory bowel disease in humans and mice, Gastroenterology 153 (2017) 550–565.
[4] U.P. Singh, N.P. Singh, B. Singh, L.J. Hofseth, R.L. Price, M. Nagarkatti, et al., Resveratrol (trans-3,5,4'-trihydroxystilbene) induces silent mating type information regulation-1 and down-regulates nuclear transcription factor-kappaB activation to abrogate dextran sulfate sodium-induced colitis, J. Pharmacol. Exp. Therapeut. 332 (2010) 829–839.
[5] X. Ma, Z. Dai, K. Sun, Y. Zhang, J. Chen, Y. Yang, et al., Intestinal epithelial cell endoplasmic reticulum stress and inflammatory bowel disease pathogenesis: an update review, Front. Immunol. 8 (2017) 1271.
[6] A. Ueno, L. Jeffery, T. Kobayashi, T. Hibi, S. Ghosh, H. Jijon, Th17 plasticity and its relevance to inflammatory bowel disease, J. Autoimmun. 87 (2018) 38–49.
[7] R. Marion-Letellier, G. Savoye, S. Ghosh, IBD: in food we trust, J Crohns Colitis 10 (2016) 1351–1361.
[8] J.K. Limdi, D. Aggarwal, J.T. McLaughlin, Dietary practices and beliefs in patients with inflammatory bowel disease, Inflamm. Bowel Dis. 22 (2016) 164–170.
[9] M. Radziszewska, J. Smarkusz-Zarzecka, L. Ostrowska, D. Pogodziński, Nutrition and supplementation in ulcerative colitis, Nutrients 14 (2022).
[10] Q.Y. Ban, M. Liu, N. Ding, Y. Chen, Q. Lin, J.M. Zha, et al., Nutraceuticals for the treatment of IBD: current progress and future directions, Front. Nutr. 9 (2022) 794169.
[11] A. Saviano, F. Raucci, G.M. Casillo, C. Indolfi, A. Pernice, C. Foreste, et al., Molecules vol. 25 (2020). Present Status and Future Trends of Natural-Derived Compounds Targeting T Helper (Th) 17 and Microsomal Prostaglandin E Synthase-1 (mPGES-1) as Alternative Therapies for Autoimmune and Inflammatory-Based Diseases.
[12] A.C. Brown, S.D. Rampertab, G.E. Mullin, Existing dietary guidelines for Crohn's disease and ulcerative colitis, Expet Rev. Gastroenterol. Hepatol. 5 (2011) 411–425.
[13] A.N. Ananthakrishnan, G.G. Kaplan, C.N. Bernstein, K.E. Burke, P.J. Lochhead, A. N. Sasson, et al., Lifestyle, behaviour, and environmental modification for the management of patients with inflammatory bowel diseases: an International Organization for Study of Inflammatory Bowel Diseases consensus, Lancet Gastroenterol Hepatol 7 (2022) 666–678.
[14] C.M. Ferreira, A.T. Vieira, M.A. Vinolo, F.A. Oliveira, R. Curi, S. Martins Fdos, The central role of the gut microbiota in chronic inflammatory diseases, J Immunol Res 2014 (2014) 689492.
[15] H. Kim, M.J. Castellon-Chicas, S. Arbizu, S.T. Talcott, N.L. Drury, S. Smith, et al., Mango (Mangifera indica L.) polyphenols: anti-inflammatory intestinal microbial health benefits, and associated mechanisms of actions, Molecules 26 (2021).
[16] S.M. Lim, J.J. Jeong, H.S. Choi, H.B. Chang, D.H. Kim, Mangiferin corrects the imbalance of Th17/Treg cells in mice with TNBS-induced colitis, Int. Immunopharm. 34 (2016) 220–228.
[17] C.L. Liang, W. Lu, J.Y. Zhou, Y. Chen, Q. Zhang, H. Liu, et al., Mangiferin attenuates murine lupus nephritis by inducing CD4+Foxp3+ regulatory T cells via suppression of mTOR signaling, Cell. Physiol. Biochem. 50 (2018) 1560–1573.
[18] W. Dou, J. Zhang, G. Ren, L. Ding, A. Sun, C. Deng, et al., Mangiferin attenuates the symptoms of dextran sulfate sodium-induced colitis in mice via NF-κB and MAPK signaling inactivation, Int. Immunopharm. 23 (2014) 170–178.
[19] S. Somani, S. Zambad, K. Modi, Mangiferin attenuates DSS colitis in mice: molecular docking and in vivo approach, Chem. Biol. Interact. 253 (2016) 18–26.
[20] A. Saviano, F. Raucci, G.M. Casillo, A.A. Mansour, V. Piccolo, C. Montesano, et al., Anti-inflammatory and immunomodulatory activity of Mangifera indica L. reveals the modulation of COX-2/mPGES-1 axis and Th17/Treg ratio, Pharmacol. Res. 182 (2022) 106283.
[21] D.V. Ostanin, J. Bao, I. Koboziev, L. Gray, S.A. Robinson-Jackson, M. Kosloski-Davidson, et al., T cell transfer model of chronic colitis: concepts, considerations, and tricks of the trade, Am. J. Physiol. Gastrointest. Liver Physiol. 296 (2009) G135–G146.
[22] M. Imran, M.S. Arshad, M.S. Butt, J.H. Kwon, M.U. Arshad, M.T. Sultan, Mangiferin: a natural miracle bioactive compound against lifestyle related disorders, Lipids Health Dis. 16 (2017) 84.
[23] A. Saviano, A.A. Manosour, F. Raucci, F. Merlino, N. Marigliano, A. Schettino, et al., New biologic (Ab-IPL-IL-17) for IL-17-mediated diseases: identification of the bioactive sequence (nIL-17) for IL-17A/F function, Ann. Rheum. Dis. 82 (2023) 1415–1428.
[24] E.M. Sturm, B. Radnai, K. Jandl, A. Stančić, G.P. Parzmair, C. Högenauer, et al., Opposing roles of prostaglandin D2 receptors in ulcerative colitis, J. Immunol. 193 (2014) 827–839.
[25] T. Lee, T. Clavel, K. Smirnov, A. Schmidt, I. Lagkouvardos, A. Walker, et al., Oral versus intravenous iron replacement therapy distinctly alters the gut microbiota and metabolome in patients with IBD, Gut 66 (2017) 863–871.
[26] V. Papandreou, N. Kavrochorianou, T. Katsoulas, P. Myrianthefs, K. Venetsanou, G. Baltopoulos, Adrenergic effect on cytokine release after ex vivo healthy volunteers' whole blood LPS stimulation, Inflammation 39 (2016) 1069–1075.
[27] S. Zheng, J. Niu, B. Geist, D. Fink, Z. Xu, H. Zhou, et al., A minimal physiologically based pharmacokinetic model to characterize colon TNF suppression and treatment effects of an anti-TNF monoclonal antibody in a mouse inflammatory bowel disease model, mAbs 12 (2020) 1813962.
[28] Z. Liu, K. Geboes, S. Colpaert, L. Overbergh, C. Mathieu, H. Heremans, et al., Prevention of experimental colitis in SCID mice reconstituted with CD45RBhigh CD4+ T cells by blocking the CD40-CD154 interactions, J. Immunol. 164 (2000) 6005–6014.
[29] G.X. Song-Zhao, K.J. Maloy, Experimental mouse models of T cell-dependent inflammatory bowel disease, Methods Mol. Biol. 1193 (2014) 199–211.
[30] P. Zhou, R. Borojevic, C. Streutker, D. Snider, H. Liang, K. Croitoru, Expression of dual TCR on DO11.10 T cells allows for ovalbumin-induced oral tolerance to prevent T cell-mediated colitis directed against unrelated enteric bacterial antigens, J. Immunol. 172 (2004) 1515–1523.
[31] Y. Mikami, T. Kanai, T. Sujino, Y. Ono, A. Hayashi, A. Okazawa, et al., Competition between colitogenic Th1 and Th17 cells contributes to the amelioration of colitis, Eur. J. Immunol. 40 (2010) 2409–2422.
[32] K. Forster, A. Goethel, C.W. Chan, G. Zanello, C. Streutker, K. Croitoru, An oral CD3-specific antibody suppresses T-cell-induced colitis and alters cytokine responses to T-cell activation in mice, Gastroenterology 143 (2012) 1298–1307.
[33] Q. He, H. Gao, Y.L. Chang, X. Wu, R. Lin, G. Li, et al., ETS-1 facilitates Th1 cell-mediated mucosal inflammation in inflammatory bowel diseases through upregulating CIRBP, J. Autoimmun. 132 (2022) 102872.
[34] K. Shimano, Y. Maeda, H. Kataoka, M. Murase, S. Mochizuki, H. Utsumi, et al., Amiselimod (MT-1303), a novel sphingosine 1-phosphate receptor-1 functional antagonist, inhibits progress of chronic colitis induced by transfer of CD4+ CD45RBhigh T cells, PLoS One 14 (2019) e0226154.
[35] M. Colucci, F. Maione, M.C. Bonito, A. Piscopo, A. Di Giannuario, S. Pieretti, New insights of dimethyl sulphoxide effects (DMSO) on experimental in vivo models of nociception and inflammation, Pharmacol. Res. 57 (2008) 419–425.
[36] T. Lindebo Holm, S.S. Poulsen, H. Markholst, S. Reedtz-Runge, Pharmacological evaluation of the SCID T cell transfer model of colitis: as a model of Crohn's disease, Int. J. Inflamm. 2012 (2012) 412178.
[37] P. Beesetty, K.B. Wieczerzak, J.N. Gibson, T. Kaitsuka, C.T. Luu, M. Matsushita, et al., Inactivation of TRPM7 kinase in mice results in enlarged spleens, reduced T-cell proliferation and diminished store-operated calcium entry, Sci. Rep. 8 (2018) 3023.
[38] L. Dong, J. Xie, Y. Wang, H. Jiang, K. Chen, D. Li, et al., Mannose ameliorates experimental colitis by protecting intestinal barrier integrity, Nat. Commun. 13 (2022) 4804.
[39] Y. Nemoto, T. Kanai, K. Kameyama, T. Shinohara, N. Sakamoto, T. Totsuka, et al., Long-lived colitogenic CD4+ memory T cells residing outside the intestine participate in the perpetuation of chronic colitis, J. Immunol. 183 (2009) 5059–5068.
[40] M. Li, J. Gao, Y. Tang, M. Liu, S. Wu, K. Qu, et al., Traditional herbal medicine-derived sulforaphene LFS-01 reverses colitis in mice by selectively altering the gut microbiota and promoting intestinal gamma-delta T cells, Front. Pharmacol. 8 (2017) 959.
[41] Q. Lv, Y. Xing, J. Liu, D. Dong, Y. Liu, H. Qiao, et al., Lonicerin targets EZH2 to alleviate ulcerative colitis by autophagy-mediated NLRP3 inflammasome inactivation, Acta Pharm. Sin. B 11 (2021) 2880–2899.
[42] P. Raju, N. Shashikanth, P.Y. Tsai, P. Pongkorpsakol, S. Chanez-Paredes, P. R. Steinhagen, et al., Inactivation of paracellular cation-selective claudin-2 channels attenuates immune-mediated experimental colitis in mice, J. Clin. Invest. 130 (2020) 5197–5208.
[43] M.Y. Song, C.P. Hong, S.J. Park, J.H. Kim, B.G. Yang, Y. Park, et al., Protective effects of Fc-fused PD-L1 on two different animal models of colitis, Gut 64 (2015) 260–271.
[44] H. Li, Y. Zhang, M. Liu, C. Fan, C. Feng, Q. Lu, et al., Targeting PDE4 as a promising therapeutic strategy in chronic ulcerative colitis through modulating mucosal homeostasis, Acta Pharm. Sin. B 12 (2022) 228–245.
[45] K. Shimizu, K. Agata, S. Takasugi, S. Goto, Y. Narita, T. Asai, et al., New strategy for MS treatment with autoantigen-modified liposomes and their therapeutic effect, J. Contr. Release 335 (2021) 389–397.
[46] F. Raucci, A. Saviano, G.M. Casillo, M. Guerra-Rodriguez, A.A. Mansour, M. Piccolo, et al., IL-17-induced inflammation modulates the mPGES-1/PPAR-γ pathway in monocytes/macrophages, Br. J. Pharmacol. 179 (2022) 1857–1873.
[47] F. Raucci, A.J. Iqbal, A. Saviano, P. Minosi, M. Piccolo, C. Irace, et al., IL-17A neutralizing antibody regulates monosodium urate crystal-induced gouty inflammation, Pharmacol. Res. 147 (2019) 104351.
[48] Y. Zhao, Y. Yang, J. Zhang, R. Wang, B. Cheng, D. Kalambhe, et al., Lactoferrin-mediated macrophage targeting delivery and patchouli alcohol-based therapeutic

strategy for inflammatory bowel diseases, Acta Pharm. Sin. B 10 (2020) 1966–1976.
[49] F. Raucci, A.J. Iqbal, A. Saviano, G.M. Casillo, M. Russo, D. Lezama, et al., In-depth immunophenotyping data relating to IL-17Ab modulation of circulating Treg/Th17 cells and of in situ infiltrated inflammatory monocytes in the onset of gouty inflammation, Data Brief 25 (2019) 104381.
[50] A. Cossarizza, H.D. Chang, A. Radbruch, S. Abrignani, R. Addo, M. Akdis, et al., Guidelines for the use of flow cytometry and cell sorting in immunological studies (third edition), Eur. J. Immunol. 51 (2021) 2708–3145.
[51] M.A. Alfwuaires, A.I. Algefare, E. Afkar, S.A. Salam, H.I.A. El-Moaty, G.M. Badr, Immunomodulatory assessment of Portulaca oleracea L. extract in a mouse model of colitis, Biomed. Pharmacother. 143 (2021) 112148.
[52] Q. Wang, C.H. Fang, P.O. Hasselgren, Intestinal permeability is reduced and IL-10 levels are increased in septic IL-6 knockout mice, Am. J. Physiol. Regul. Integr. Comp. Physiol. 281 (2001) R1013–R1023.
[53] Y. Wang, B. Wei, D. Wang, J. Wu, J. Gao, H. Zhong, et al., DNA damage repair promotion in colonic epithelial cells by andrographolide downregulated cGAS–STING pathway activation and contributed to the relief of CPT-11-induced intestinal mucositis, Acta Pharm. Sin. B 12 (2022) 262–273.
[54] M. Cui, A. Trimigno, V. Aru, B. Khakimov, S.B. Engelsen, Human faecal (1)H NMR metabolomics: evaluation of solvent and sample processing on coverage and reproducibility of signature metabolites, Anal. Chem. 92 (2020) 9546–9555.
[55] L.E. Romick-Rosendale, A.M. Goodpaster, P.J. Hanwright, N.B. Patel, E. T. Wheeler, D.L. Chona, et al., NMR-based metabonomics analysis of mouse urine and fecal extracts following oral treatment with the broad-spectrum antibiotic enrofloxacin (Baytril), Magn. Reson. Chem. 47 (Suppl 1) (2009) S36–S46.
[56] Y.S. Hong, Y.T. Ahn, J.C. Park, J.H. Lee, H. Lee, C.S. Huh, et al., 1H NMR-based metabonomic assessment of probiotic effects in a colitis mouse model, Arch Pharm. Res. (Seoul) 33 (2010) 1091–1101.
[57] F. Savorani, G. Tomasi, S. B. Engelsen icoshift, A versatile tool for the rapid alignment of 1D NMR spectra, J. Magn. Reson. 202 (2010) 190–202.
[58] C. Cristiano, F. Volpicelli, P. Lippiello, B. Buono, F. Raucci, M. Piccolo, et al., Neutralization of IL-17 rescues amyloid-β-induced neuroinflammation and memory impairment, Br. J. Pharmacol. 176 (2019) 3544–3557.
[59] G. Ercolano, A. Gomez-Cadena, N. Dumauthioz, G. Vanoni, M. Kreutzfeldt, T. Wyss, et al., PPARγ drives IL-33-dependent ILC2 pro-tumoral functions, Nat. Commun. 12 (2021) 2538.
[60] H.M. McGettrick, L.M. Butler, G.B. Nash, Analysis of leukocyte migration through monolayers of cultured endothelial cells, Methods Mol. Biol. 370 (2007) 37–54.
[61] S.P. Tull, C.M. Yates, B.H. Maskrey, V.B. O'Donnell, J. Madden, R.F. Grimble, et al., Omega-3 Fatty acids and inflammation: novel interactions reveal a new step in neutrophil recruitment, PLoS Biol. 7 (2009) e1000177.
[62] H.M. McGettrick, K. Hunter, P.A. Moss, C.D. Buckley, G.E. Rainger, G.B. Nash, Direct observations of the kinetics of migrating T cells suggest active retention by endothelial cells with continual bidirectional migration, J. Leukoc. Biol. 85 (2009) 98–107.
[63] S.R. Ahmed, H.M. McGettrick, C.M. Yates, C.D. Buckley, M.J. Ratcliffe, G.B. Nash, et al., Prostaglandin D2 regulates CD4+ memory T cell trafficking across blood vascular endothelium and primes these cells for clearance across lymphatic endothelium, J. Immunol. 187 (2011) 1432–1439.
[64] A.A. Mansour, F. Raucci, M. Sevim, A. Saviano, J. Begum, Z. Zhi, et al., Galectin-9 supports primary T cell transendothelial migration in a glycan and integrin dependent manner, Biomed. Pharmacother. 151 (2022) 113171.
[65] A. Saviano, G.M. Casillo, F. Raucci, A. Pernice, C. Santarcangelo, M. Piccolo, et al., Supplementation with ribonucleotide-based ingredient (Ribodiet®) lessens oxidative stress, brain inflammation, and amyloid pathology in a murine model of Alzheimer, Biomed. Pharmacother. 139 (2021) 111579.
[66] A. Saviano, S. De Vita, M.G. Chini, N. Marigliano, G. Lauro, G.M. Casillo, et al., Silico, in vitro, and in vivo analysis of tanshinone IIA and cryptotanshinone from salvia miltiorrhiza as modulators of cyclooxygenase-2/mPGES-1/endothelial prostaglandin EP3 pathway, Biomolecules 12 (2022).
[67] F. Caso, A. Saviano, M. Tasso, F. Raucci, N. Marigliano, S. Passavanti, et al., Analysis of rheumatoid- vs psoriatic arthritis synovial fluid reveals differential macrophage (CCR2) and T helper subsets (STAT3/4 and FOXP3) activation, Autoimmun. Rev. 21 (2022) 103207.
[68] V. Vellecco, A. Saviano, F. Raucci, G.M. Casillo, A.A. Mansour, E. Panza, et al., Interleukin-17 (IL-17) triggers systemic inflammation, peripheral vascular dysfunction, and related prothrombotic state in a mouse model of Alzheimer's disease, Pharmacol. Res. 187 (2023) 106595.
[69] F. Maione, N. Paschalidis, N. Mascolo, N. Dufton, M. Perretti, F. D'Acquisto, Interleukin 17 sustains rather than induces inflammation, Biochem. Pharmacol. 77 (2009) 878–887.
[70] F. Maione, A.J. Iqbal, F. Raucci, M. Letek, M. Bauer, F. D'Acquisto, Repetitive exposure of IL-17 into the murine air pouch favors the recruitment of inflammatory monocytes and the release of IL-16 and TREM-1 in the inflammatory fluids, Front. Immunol. 9 (2018) 2752.
[71] L. Wang, D. Yao, R. Deepak, H. Liu, Q. Xiao, H. Fan, et al., Structures of the human PGD(2) receptor CRTH2 reveal novel mechanisms for ligand recognition, Mol. Cell 72 (2018) 48–59.e4.
[72] J.L. Banks, H.S. Beard, Y. Cao, A.E. Cho, W. Damm, R. Farid, et al., Integrated modeling program, applied chemical theory (IMPACT), J. Comput. Chem. 26 (2005) 1752–1780.
[73] R.A. Friesner, R.B. Murphy, M.P. Repasky, L.L. Frye, J.R. Greenwood, T. A. Halgren, et al., Extra precision glide: docking and scoring incorporating a model of hydrophobic enclosure for protein-ligand complexes, J. Med. Chem. 49 (2006) 6177–6196.
[74] T.A. Halgren, R.B. Murphy, R.A. Friesner, H.S. Beard, L.L. Frye, W.T. Pollard, et al., Glide: a new approach for rapid, accurate docking and scoring. 2. Enrichment factors in database screening, J. Med. Chem. 47 (2004) 1750–1759.
[75] J. Torres, S. Mehandru, J.F. Colombel, L. Peyrin-Biroulet, Crohn's disease, Lancet 389 (2017) 1741–1755.
[76] L. Belarif, R. Danger, L. Kermarrec, V. Nerrière-Daguin, S. Pengam, T. Durand, et al., IL-7 receptor influences anti-TNF responsiveness and T cell gut homing in inflammatory bowel disease, J. Clin. Invest. 129 (2019) 1910–1925.
[77] M. Allez, K. Karmiris, E. Louis, G. Van Assche, S. Ben-Horin, A. Klein, et al., Report of the ECCO pathogenesis workshop on anti-TNF therapy failures in inflammatory bowel diseases: definitions, frequency and pharmacological aspects, J Crohns Colitis 4 (2010) 355–366.
[78] J.A. Tibble, G. Sigthorsson, R. Foster, I. Forgacs, I. Bjarnason, Use of surrogate markers of inflammation and Rome criteria to distinguish organic from nonorganic intestinal disease, Gastroenterology 123 (2002) 450–460.
[79] C. Gentile, A. Perrone, A. Attanzio, L. Tesoriere, M.A. Livrea, Sicilian pistachio (Pistacia vera L.) nut inhibits expression and release of inflammatory mediators and reverts the increase of paracellular permeability in IL-1β-exposed human intestinal epithelial cells, Eur. J. Nutr. 54 (2015) 811–821.
[80] W. Stremmel, S. Staffer, M.J. Schneider, H. Gan-Schreier, A. Wannhoff, N. Stuhrmann, et al., Genetic mouse models with intestinal-specific tight junction deletion resemble an ulcerative colitis phenotype, J Crohns Colitis 11 (2017) 1247–1257.
[81] A.G. Røseth, P.N. Schmidt, M.K. Fagerhol, Correlation between faecal excretion of indium-111-labelled granulocytes and calprotectin, a granulocyte marker protein, in patients with inflammatory bowel disease, Scand. J. Gastroenterol. 34 (1999) 50–54.
[82] S. Mehandru, J.F. Colombel, The intestinal barrier, an arbitrator turned provocateur in IBD, Nat. Rev. Gastroenterol. Hepatol. 18 (2021) 83–84.
[83] E.A. Franzosa, A. Sirota-Madi, J. Avila-Pacheco, N. Fornelos, H.J. Haiser, S. Reinker, et al., Author Correction: gut microbiome structure and metabolic activity in inflammatory bowel disease, Nat Microbiol 4 (2019) 898.
[84] E.C. Rosser, C.J.M. Piper, D.E. Matei, P.A. Blair, A.F. Rendeiro, M. Orford, et al., Microbiota-derived metabolites suppress arthritis by amplifying aryl-hydrocarbon receptor activation in regulatory B cells, Cell Metabol. 31 (2020) 837–851.e10.
[85] M.R. Nicholson, E. Alexander, S. Ballal, Z. Davidovics, M. Docktor, M. Dole, et al., Efficacy and outcomes of faecal microbiota transplantation for recurrent clostridioides difficile infection in children with inflammatory bowel disease, J Crohns Colitis 16 (2022) 768–777.
[86] W. Yang, Y. Cong, Exploring colitis through dynamic T cell adoptive transfer models, Inflamm. Bowel Dis. 29 (2023) 1673–1680.
[87] S. Negi, S. Saini, N. Tandel, K. Sahu, R.P.N. Mishra, R.K. Tyagi, Translating Treg therapy for inflammatory bowel disease in humanized mice, Cells 10 (2021).
[88] A.M. Mowat, Anatomical basis of tolerance and immunity to intestinal antigens, Nat. Rev. Immunol. 3 (2003) 331–341.
[89] T.W. Spahn, T. Kucharzik, Modulating the intestinal immune system: the role of lymphotoxin and GALT organs, Gut 53 (2004) 456–465.
[90] F.M. Marelli-Berg, L. Cannella, F. Dazzi, V. Mirenda, The highway code of T cell trafficking, J. Pathol. 214 (2008) 179–189.
[91] F.M. Marelli-Berg, H. Fu, F. Vianello, K. Tokoyoda, A. Hamann, Memory T-cell trafficking: new directions for busy commuters, Immunology 130 (2010) 158–165.
[92] J.P. Pereira, L.M. Kelly, J.G. Cyster, Finding the right niche: B-cell migration in the early phases of T-dependent antibody responses, Int. Immunol. 22 (2010) 413–419.
[93] F. Maione, G.M. Casillo, F. Raucci, A.J. Iqbal, N. Mascolo, The functional link between microsomal prostaglandin E synthase-1 (mPGES-1) and peroxisome proliferator-activated receptor γ (PPARγ) in the onset of inflammation, Pharmacol. Res. 157 (2020) 104807.
[94] M.D. Salvado, A. Alfranca, A. Escolano, J.Z. Haeggström, J.M. Redondo, COX-2 limits prostanoid production in activated HUVECs and is a source of PGH2 for transcellular metabolism to PGE2 by tumor cells, Arterioscler. Thromb. Vasc. Biol. 29 (2009) 1131–1137.
[95] K. Casós, L. Siguero, M.T. Fernández-Figueras, X. León, M.P. Sardá, L. Vila, et al., Tumor cells induce COX-2 and mPGES-1 expression in microvascular endothelial cells mainly by means of IL-1 receptor activation, Microvasc. Res. 81 (2011) 261–268.
[96] M. Soler, M. Camacho, J.R. Escudero, M.A. Iñiguez, L. Vila, Human vascular smooth muscle cells but not endothelial cells express prostaglandin E synthase, Circ. Res. 87 (2000) 504–507.
[97] I.F. Charo, S. Shak, M.A. Karasek, P.M. Davison, I.M. Goldstein, Prostaglandin I2 is not a major metabolite of arachidonic acid in cultured endothelial cells from human foreskin microvessels, J. Clin. Invest. 74 (1984) 914–919.
[98] D.A. Sandham, L. Barker, L. Brown, Z. Brown, D. Budd, S.J. Charlton, et al., Discovery of fevipiprant (NVP-QAW039), a potent and selective DP(2) receptor antagonist for treatment of asthma, ACS Med. Chem. Lett. 8 (2017) 582–586.
[99] H. Sugimoto, M. Shichijo, T. Iino, Y. Manabe, A. Watanabe, M. Shimazaki, et al., An orally bioavailable small molecule antagonist of CRTH2, ramatroban (BAY u3405), inhibits prostaglandin D2-induced eosinophil migration in vitro, J. Pharmacol. Exp. Therapeut. 305 (2003) 347–352.
[100] C.N. Serhan, Pro-resolving lipid mediators are leads for resolution physiology, Nature 510 (2014) 92–101.